

# On the Emergence of Induction Heads for In-Context Learning

Tiberiu Musat\*    Tiago Pimentel    Lorenzo Noci    Alessandro Stolfo  
Mrinmaya Sachan    Thomas Hofmann  
ETH Zürich

## Abstract

Transformers have become the dominant architecture for natural language processing. Part of their success is owed to a remarkable capability known as *in-context learning* (ICL): they can acquire and apply novel associations solely from their input context, without any updates to their weights. In this work, we study the emergence of *induction heads*, a previously identified mechanism in two-layer transformers that is particularly important for in-context learning. We uncover a relatively simple and interpretable structure of the weight matrices implementing the induction head. We theoretically explain the origin of this structure using a minimal ICL task formulation and a modified transformer architecture. We give a formal proof that the training dynamics remain constrained to a 19-dimensional subspace of the parameter space. Empirically, we validate this constraint while observing that only 3 dimensions account for the emergence of an induction head. By further studying the training dynamics inside this 3-dimensional subspace, we find that the time until the emergence of an induction head follows a tight asymptotic bound that is quadratic in the input context length.

## 1 Introduction

LLMs possess a remarkable ability known as *in-context learning* (ICL). A well-trained language model can learn and apply novel associations from their input context, without additional parameter updates (Brown et al., 2020).

Previous work by Olsson et al. (2022) traces back transformers’ ICL capabilities to a learned mechanism termed *induction head*: a pair of attention heads that implement a simple but powerful copying rule  $[\dots, A, B, \dots, A] \rightarrow B$ . Empirical work has shown that the emergence of induction heads co-occurs with a sharp decrease in the train-

ing loss and an increase in ICL accuracy (Olsson et al., 2022; Reddy, 2023).

Reddy (2023) has proposed a three-parameter model of the induction head that can successfully account for the phenomena of abrupt learning and data distributional effects. However, the three parameters are inspired by the attention patterns of an induction head without a clear connection to the learned weights of a transformer. On the other hand, existing theoretical works that study the evolution of the weights during training are limited to simplified staged learning algorithms (Nichani et al., 2024; Bietti et al., 2024).

Our work aims to illuminate the precise training dynamics during the emergence of induction heads. To answer this question, we study the training dynamics of an autoregressive two-layer transformer using a minimal in-context learning task and a simplified architecture. We uncover a precise description of the model weights during training and a tight bound on the learning time.

Concretely, our contributions are as follows:

1. Using a minimal ICL formulation, we give a formal proof that training dynamics induce a simplified structure of the weights (Section 3.2). The evolution of model weights stays within a 19-dimensional subspace of the entire parameter space, regardless of model or task size. We index this subspace by introducing **19 pseudo-parameters**.
2. We empirically find that only **3 pseudo-parameters** are learned at the end of training, corresponding exactly to an induction head (Section 3.3). We also find that the emergence of the 3 parameters is *self-contained*, unaided by the presence of the other 16 parameters.
3. We theoretically study the training dynamics of the induction head, assuming that only the 3 parameters are learnable (Section 3.4). We prove that the 3 parameters always emerge in

\*Corresponding author. Email: tmusat@ethz.ch.

a specific sequence. We also prove asymptotic bounds for the emergence time for each parameter in terms of the context length and a **tight bound on the total emergence time**.

4. We train and interpret a standard attention-only transformer on an ICL task (Section 4). We find a relatively simple **description of the weight matrices** that implement the induction head. Using progress measures during training, we show that the emergence of induction heads in standard transformers closely resembles the minimal model.

Finally, we also provide empirical validation for our theoretical results.

## 2 Transformers and Induction Heads

An essential feature of natural language is the presence of *reoccurring associations*. These can be as simple as repeated groups of words, such as the full names of people (e.g. ‘‘Alan Turing’’) or even the repeated occurrence of the phrase ‘‘induction heads’’ in this very document. However, we also observe the reoccurrence of very abstract associations, a phenomenon related to *in-context learning*. Specific examples include fact retrieval, translation, and pattern matching (Olsson et al., 2022).

Let  $\mathbf{v} \in \mathcal{V}^*$  be a sequence of tokens in a language model’s vocabulary  $\mathcal{V}$ . In language modeling, our goal is typically to characterize the distribution  $p_{\theta}(v_t | \mathbf{v}_{<t})$ . Typically, this is implemented in a transformer via a series of operations. First, we map a model’s input tokens  $\mathbf{v}_{<t}$  to embeddings  $\mathbf{X} \in \mathbb{R}^{d \times t}$ ; this is done via a lookup operation:

$$\mathbf{X} = \text{LookUp}(\mathbf{v}_{<t}) \quad (1)$$

Afterwards, the model implements a series of self-attention operations:

$$\mathbf{H}^{\ell} = \text{SelfAttention}(\mathbf{H}^{\ell-1}) \quad (2)$$

where, by definition,  $\mathbf{H}^0 = \mathbf{X}$ . Finally, in a last layer, the model predicts the next token as:

$$p_{\theta}(v_t | \mathbf{v}_{<t}) = \text{softmax}(\mathbf{W}_{\text{unemb}} \mathbf{H}^L) \quad (3)$$

where  $\mathbf{W}_{\text{unemb}} \in \mathbb{R}^{|\mathcal{V}| \times d}$  is known as an unembedding matrix.

If a pair of tokens appears in the language model’s context  $\mathbf{v}_{<t}$  as  $v_{t'}v_{t'+1} = ab$ , this pair is more likely than chance to appear again; when we have  $v_{t-1} = a$ , we may thus want to predict  $b$  as our next token in  $p_{\theta}(v_t | \mathbf{v}_{<t})$ .

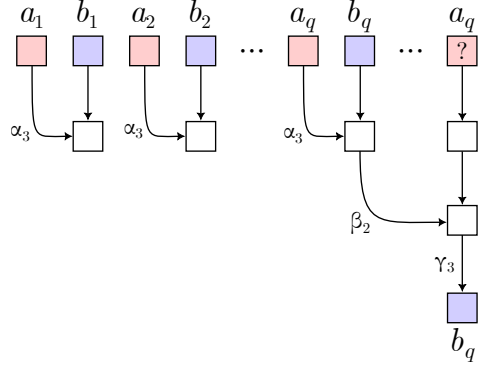


Figure 1: An induction head solving the *in-context learning* (ICL) task. Given a series of item-label pairs, the model predicts the correct label for a query item. The first attention head retrieves the corresponding item for each label, enabling the second attention head to retrieve the correct label. Each path is modulated by one pseudo-parameter ( $\alpha_3$ ,  $\beta_2$ , or  $\gamma_3$ ).

**Induction heads** are a specific structure inside transformers that implements exactly this copying behavior. Given a prompt of the form  $\dots ab \dots a$ , an induction head predicts the token which follows the previous occurrence of  $a$ , in this case being  $b$ . Note that induction heads are not a modified type of attention head, but rather a mechanism learned by regular attention heads during standard training.

We wish to, after observing  $v_{t-1} = v_{t'}$ , copy the value of  $v_{t'+1}$  into  $v_t$ . Due to the structure of self-attention, however, this requires at least two steps (Sanford et al., 2024). First, the model must copy the token information from position  $t'$  into  $t' + 1$ . Second, the newly obtained value enables the model to attend to position  $t' + 1$  from  $t - 1$ .

## 3 Induction Heads in Simplified Transformers

### 3.1 Disentangled Transformer

In order to understand the emergence of induction heads, we study the training dynamics in a minimal formulation. We propose a simplified, but equally powerful, transformer architecture (depicted in Figure 2) with a *disentangled* residual stream (Friedman et al., 2023).

#### 3.1.1 Data Distribution

We use a common ICL task formulation that requires labeling an item based on a list of  $N$  item-label pairs (Chan et al., 2022; Reddy, 2023; Hochreiter et al., 2001). The  $i^{\text{th}}$  pair consists of an item  $\mathbf{a}_i \in \mathbb{R}^D$  and a label  $\mathbf{b}_i \in \mathbb{R}^D$  with dimensionality

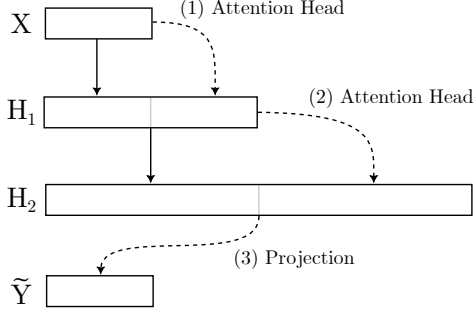


Figure 2: Our minimal transformer architecture. We use two attention-only layers and a linear layer; we disentangle the attention layers by concatenating the inputs and outputs, rather than adding them together.

$D \in \mathbb{N}$ . We ask the model to predict the label for one of the items  $\mathbf{a}_q$  where  $q \in \{1, \dots, N\}$ .

We annotate each item with a positional embedding  $\mathbf{p}_i \in \mathbb{R}^D$  and each label with the rotated positional embedding  $\mathbf{M}\mathbf{p}_i$ , where  $\mathbf{M} \in \mathbb{R}^{D \times D}$ . The rotation is fixed before training to create a learnable correlation similar to a sinusoidal embedding (Vaswani et al., 2017). This enables the attention mechanism to connect the corresponding items and labels. We do not use any positional embedding for the query item. Assuming that  $D$  is even, we use

$$\mathbf{M} = \left[ \begin{array}{c|c} \mathbf{0}_{(D/2) \times (D/2)} & \mathbf{I}_{D/2} \\ \hline \mathbf{I}_{D/2} & \mathbf{0}_{(D/2) \times (D/2)} \end{array} \right], \quad (4)$$

where  $\mathbf{I}_{D/2} \in \mathbb{R}^{(D/2) \times (D/2)}$  is the identity matrix.

We concatenate items and labels with their positional embeddings to obtain our data:

$$\mathbf{X}_{2i-1,:} = [\mathbf{a}_i^\top \mid \mathbf{p}_i^\top]^\top \quad \mathbf{X}_{2i,:} = [\mathbf{b}_i^\top \mid \mathbf{p}_i^\top \mathbf{M}]^\top \\ \forall i \in \{1, \dots, N\}$$

$$\mathbf{X}_{2N+1,:} = [\mathbf{a}_q^\top \mid \mathbf{0}]^\top \quad \mathbf{y} = \mathbf{b}_q \\ q \in \{1, \dots, N\}$$

where  $\mathbf{X} \in \mathbb{R}^{(2N+1) \times 2D}$ ,  $\mathbf{y} \in \mathbb{R}^D$ , and  $[\cdot \mid \cdot]$  denotes concatenation.

We assume a *lexinvariant* language model (Huang et al., 2023) where items, labels, and positional embeddings are independent and identically distributed. For our theoretical results, we introduce additional assumptions on the distribution of items, labels, and positional embeddings, as needed.

We train our model with mean-squared error loss  $\mathcal{L} = \|\mathbf{y} - \tilde{\mathbf{y}}\|^2$  using only the output of the query item located at the last position, i.e.  $\tilde{\mathbf{y}} = \tilde{\mathbf{Y}}_{2N+1,:}$ .

### 3.1.2 Architecture

Our transformer has two single-head attention layers followed by a linear layer. For the attention layers, we use a merged key-query matrix and no value/projection matrix. We disentangle the residual stream by directly concatenating the attention output to the existing residual stream:

$$\mathbf{H}_1 = \left[ \mathbf{X} \mid \sigma(\mathbf{X}\mathbf{W}^{(1)}\mathbf{X}^\top) \mathbf{X} \right], \quad (5)$$

$$\mathbf{H}_2 = \left[ \mathbf{H}_1 \mid \sigma(\mathbf{H}_1\mathbf{W}^{(2)}\mathbf{H}_1^\top) \mathbf{H}_1 \right], \quad (6)$$

$$\tilde{\mathbf{Y}} = \mathbf{H}_2\mathbf{W}^{(3)}, \quad (7)$$

where  $[\cdot \mid \cdot]$  denotes matrix concatenation and  $\sigma$  denotes the softmax function with autoregressive masking.  $\mathbf{W}^{(1)} \in \mathbb{R}^{2D \times 2D}$ ,  $\mathbf{W}^{(2)} \in \mathbb{R}^{4D \times 4D}$ ,  $\mathbf{W}^{(3)} \in \mathbb{R}^{8D \times D}$  are the learnable weights and  $\mathbf{H}_1 \in \mathbb{R}^{(2N+1) \times 4D}$ ,  $\mathbf{H}_2 \in \mathbb{R}^{(2N+1) \times 8D}$ ,  $\tilde{\mathbf{Y}} \in \mathbb{R}^{(2N+1) \times D}$  denote the activations and final output.

**Justification.** Merged key-query matrices are commonly used in theoretical works (Edelman et al., 2024; Nichani et al., 2024). We do not use MLPs since they are neither necessary nor useful for the task at hand. The disentangled transformer has the same expressivity as a regular transformer with a large residual dimension.

### 3.2 Training Dynamics

Our model has a total of  $28D^2$  parameters. However, as we show below, the training dynamics on our data distribution remain constrained to a 19-dimensional subspace that we index using 19 pseudo-parameters. Our theoretical result is based on the following assumptions:

**Assumption 1. Zero Initialization.** We assume our neural network is initialized with zero weights, i.e.  $\mathbf{W}^{(1)} = \mathbf{0}$ ,  $\mathbf{W}^{(2)} = \mathbf{0}$ , and  $\mathbf{W}^{(3)} = \mathbf{0}$ .

The zero initialization is commonly used in theoretical works (Nichani et al., 2024; Edelman et al., 2024), being motivated as a reasonable approximation for small random initializations.

**Assumption 2. Population Loss.** We assume the network is trained with gradient descent over the entire data distribution at every step:

$$\mathbf{W}^{(k)} \leftarrow \mathbf{W}^{(k)} - \lambda \mathbb{E} \left[ \frac{\partial \mathcal{L}}{\partial \mathbf{W}^{(k)}} \right], \quad (8)$$

where  $\lambda > 0$  is the learning rate.

**Assumption 3. Isotropic Data.** We assume that the data distribution is invariant to orthogonal transformations of items, labels, and positional embeddings:

$$\begin{aligned} f(\{\mathbf{a}_i\}, \{\mathbf{b}_i\}, \{\mathbf{p}_i\}, q) & \quad (9) \\ &= f(\{\mathbf{E}\mathbf{a}_i\}, \{\mathbf{E}\mathbf{b}_i\}, \{\mathbf{p}_i\}, q) \\ &= f(\{\mathbf{a}_i\}, \{\mathbf{b}_i\}, \{\mathbf{E}\mathbf{p}_i\}, q), \end{aligned}$$

for any orthogonal matrix  $\mathbf{E} \in \mathbb{R}^{D \times D}$ , where  $f(\{\mathbf{a}_i\}, \{\mathbf{b}_i\}, \{\mathbf{p}_i\}, q)$  is the probability density over the items, labels, positional embeddings, and query index.

Note that this assumption is weaker than, for example, assuming a normal distribution, since a normal distribution is isotropic.

**Theorem 1.** Assume that we train a disentangled transformer from zero initialization with population loss on isotropic data on our ICL task. Then, the weight matrices will have the following structure throughout the entire training process:

$$\mathbf{W}^{(1)} = \left[ \begin{array}{c|c} \alpha_1 \mathbf{I} & \mathbf{0} \\ \hline \mathbf{0} & \alpha_2 \mathbf{I} + \alpha_3 \mathbf{M} \end{array} \right],$$

$$\mathbf{W}^{(2)} = \left[ \begin{array}{c|c|c|c} \beta_1 \mathbf{I} & \mathbf{0} & \beta_2 \mathbf{I} & \mathbf{0} \\ \hline \mathbf{0} & \beta_3 \mathbf{I} + \beta_4 \mathbf{M} & \mathbf{0} & \beta_5 \mathbf{I} + \beta_6 \mathbf{M} \\ \hline \beta_7 \mathbf{I} & \mathbf{0} & \beta_8 \mathbf{I} & \mathbf{0} \\ \hline \mathbf{0} & \beta_9 \mathbf{I} + \beta_{10} \mathbf{M} & \mathbf{0} & \beta_{11} \mathbf{I} + \beta_{12} \mathbf{M} \end{array} \right],$$

$$\mathbf{W}^{(3)} = \left[ \begin{array}{c|c|c|c|c} \gamma_1 \mathbf{I} & \mathbf{0} & \gamma_2 \mathbf{I} & \mathbf{0} & \gamma_3 \mathbf{I} & \mathbf{0} & \gamma_4 \mathbf{I} & \mathbf{0} \end{array} \right]^\top,$$

where we collect the parameters of each weight matrix in three vectors  $\alpha \in \mathbb{R}^3$ ,  $\beta \in \mathbb{R}^{12}$  and  $\gamma \in \mathbb{R}^4$  that vary throughout training.

*Proof Sketch.* We give an inductive proof by showing that, if weights have the above structure, then their gradients also have the same structure. Since the zero initialization fits the structure, this ensures that the structure is preserved during training.

To prove the structure of the gradient, we apply a carefully chosen rotation to the entire data distribution. Since the data distribution is isotropic, the rotation will not change the data distribution, so the expected gradient will also remain unchanged.

However, we are also able to show that our rotation induces a specific similarity transformation of the gradient:

$$\mathbb{E} \left[ \frac{\partial \mathcal{L}}{\partial \mathbf{W}_{ij}^{(k)}} \right] = F \mathbb{E} \left[ \frac{\partial \mathcal{L}}{\partial \mathbf{W}_{ij}^{(k)}} \right] F^\top, \quad (10)$$

where  $F$  is an orthogonal or block-orthogonal matrix and  $\mathbf{W}_{ij}^{(k)}$  is a block of a weight matrix. From this, we are able to show that the expected gradient must have the desired structure. We give the full proof in Section A.  $\square$

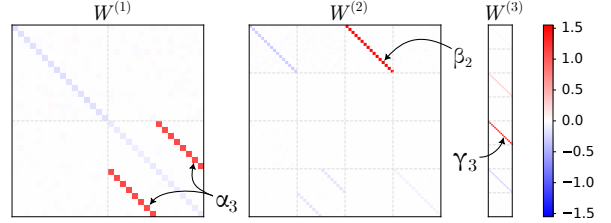


Figure 3: Weights at the end of standard training have the theoretically predicted structure.

**Empirical Validation.** In Figure 3, we confirm our theoretical result by visualizing the weights at the end of training with stochastic gradient descent. We provide the full training details and additional figures in Section C.

### 3.3 Emergence of Induction Heads

We now proceed to studying the evolution of these 19 pseudo-parameters during training. By observing or ablating specific parameters, we are able to test two hypotheses regarding the emergence of induction heads.

**Hypothesis 1** (due to Olsson et al. (2022)). *Induction Head Phase Transition.* Reaching low training loss on our ICL task coincides with the emergence of an induction head.

We can already see from Figure 3 that three parameters have a larger magnitude, namely  $\alpha_3$ ,  $\beta_2$ , and  $\gamma_3$ . Interestingly, the mechanism performed by these three parameters together corresponds exactly to an induction head. In the first layer,  $\alpha_3$  makes each label attend to the preceding item. In the second layer,  $\beta_2$  makes the query item attend to the correct label based on the newly retrieved item. Finally,  $\gamma_3$  outputs the label retrieved by the second layer. In Figure 4, we visualize the 19 pseudo-parameters and loss during training, confirming that the drop in loss is driven by the emergence of the induction head.

**Hypothesis 2. Self-Contained Dynamics.** The emergence of the induction head is unaided by the presence of any other parameter.

By training the model while constraining its parameters to the 3-dimensional subspace spanned

by the three parameters, we uncover very similar dynamics. As depicted in Figure 5, we find that the emergence of the induction head is unaffected, even slightly accelerated. We show a few more plots and full training details in Section D.

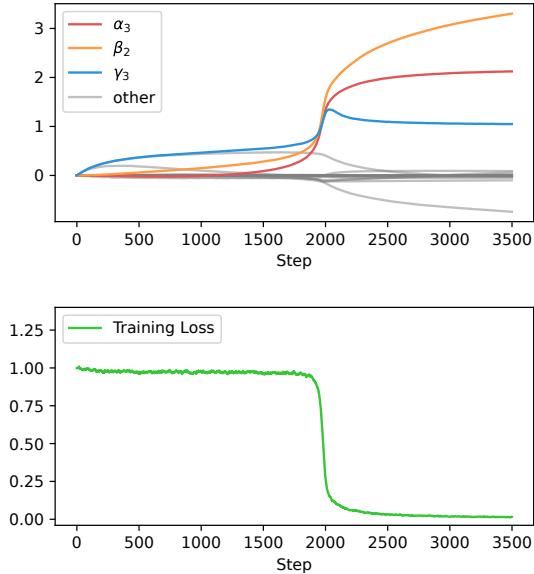


Figure 4: The value of the 19 pseudo-parameters during training (*top*) and the associated training loss (*bottom*).

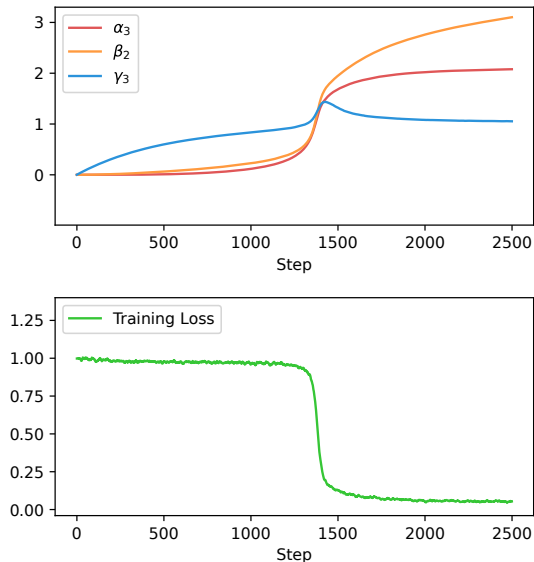


Figure 5: Ablating all parameters except  $\alpha_3$ ,  $\beta_2$ , and  $\gamma_3$  results in strikingly similar dynamics.

### 3.4 Training Dynamics of Induction Heads

Motivated by the empirical results in the previous section, we study the training dynamics constrained to the 3-dimensional subspace spanned by  $\alpha_3$ ,  $\beta_2$ , and  $\gamma_3$ , finding several tight bounds for the emer-

gence of the induction head. Specifically, we have the following assumptions:

**Assumption 4. Three-Parameter Model.** Only parameters  $\alpha_3$ ,  $\beta_2$ , and  $\gamma_3$  are learnable.

**Assumption 5. Gradient Flow.** We study the training dynamics under the assumption of a continuous-time gradient flow with unit learning rate,

$$\frac{\partial \alpha_3}{\partial t} = -\frac{\partial \mathcal{L}}{\partial \alpha_3}, \quad \frac{\partial \beta_2}{\partial t} = -\frac{\partial \mathcal{L}}{\partial \beta_2}, \quad \frac{\partial \gamma_3}{\partial t} = -\frac{\partial \mathcal{L}}{\partial \gamma_3},$$

where  $\alpha_3, \beta_2, \gamma_3 : \mathbb{R}_{\geq 0} \rightarrow \mathbb{R}$  are the continuous-time trajectories of the three parameters.

**Assumption 6. Zero Initialization.** We assume our neural network is initialized with zero weights. Equivalently,  $\alpha_3(0) = \beta_2(0) = \gamma_3(0) = 0$ .

**Assumption 7. Orthonormal Inputs.** We assume that all items, labels, and positional embeddings are orthogonal and have unit norm. Specifically,

$$\|\mathbf{a}_i\| = \|\mathbf{b}_i\| = \|\mathbf{p}_i\| = 1, \quad (11)$$

$$\mathbf{a}_i^\top \mathbf{a}_j = \mathbf{b}_i^\top \mathbf{b}_j = \mathbf{a}_i^\top \mathbf{b}_i = 0, \quad (12)$$

$$\mathbf{p}_i^\top \mathbf{p}_j = \mathbf{p}_i^\top \mathbf{M} \mathbf{p}_i = \mathbf{p}_i^\top \mathbf{M} \mathbf{p}_j = 0, \quad (13)$$

for all  $i, j \in \{1, 2, \dots, N\}, i \neq j$ .

Note that this assumption requires  $D \geq 2N$ . There are two ways to motivate this assumption, either by preprocessing the inputs using a whitening transformation, or by considering a very large dimension  $D \rightarrow \infty$  and vectors sampled from an i.i.d. Gaussian with variance  $1/\sqrt{D}$ .

**Assumption 8. Query Last.** We assume that the query item always refers to the last item-label pair present in the sequence, or  $q = N$ .

Note that even if the target label’s position is fixed, a full induction head is still required: the model cannot directly attend to specific positions because positional embeddings are randomly generated and carry no explicit location information.

**Definition 1. Parameter Emergence Time.** We say that each of the parameters  $\alpha$ ,  $\beta$ , or  $\gamma$  has emerged when its value becomes greater than  $1/2$  for the first time:

$$T_\alpha = \inf \left\{ t \mid \alpha_3(t) \geq \frac{1}{2} \right\}, \quad (14)$$

$$T_\beta = \inf \left\{ t \mid \beta_2(t) \geq \frac{1}{2} \right\}, \quad (15)$$

$$T_\gamma = \inf \left\{ t \mid \gamma_3(t) \geq \frac{1}{2} \right\}, \quad (16)$$

where  $t \in \mathbb{R}_{\geq 0}$ .

**Theorem 2.** Assume that inputs are orthonormal and that only parameters  $\alpha_3, \beta_2$ , and  $\gamma_3$  are learnable. In this case, for large enough  $N$ , parameters always emerge in the order  $T_\gamma < T_\beta < T_\alpha$  and the emergence times asymptotically follow:

$$T_\alpha = \Theta(N^2), \quad T_\beta = \Theta(N^2), \quad T_\gamma = \Theta(N),$$

with  $N$  item-label pairs in the context.

*Proof Sketch.* The proof is based on proving bounds for the gradient of each parameter. Before the emergence of any parameter, we have that  $\partial\gamma_3/\partial t = \Theta(1/N)$ , while  $\partial\alpha_3/\partial t = O(1/N^2)$  and  $\partial\beta_2/\partial t = O(1/N^2)$ . This implies that  $\gamma_3$  emerges first in  $\Theta(N)$ . Afterwards, we show that  $\partial\beta_2/\partial t = \Theta(1/N^2)$  and  $\partial\beta_2/\partial t > \partial\alpha_3/\partial t$ . This implies that  $\beta_2$  emerges next in  $\Theta(N^2)$ . Finally, we show that  $\partial\alpha_3/\partial t = o(1/N^2)$ , which implies that  $\alpha_3$  emerges last in  $\Theta(N^2)$ . See the full proof in Section B.  $\square$

**Definition 2. Induction Head.** We say that an induction head has emerged if all three parameters are greater than  $1/2$ .

**Definition 3. Time until ICL.** We say that in-context learning has emerged at the first time when the induction head is present. Specifically,

$$t_{ICL} = \inf \left\{ t \mid \min(\alpha_3(t), \beta_2(t), \gamma_3(t)) \geq \frac{1}{2} \right\}.$$

**Corollary 1.** The time until the emergence of in-context learning asymptotically follows:

$$t_{ICL} = \Theta(N^2),$$

where  $N$  is the number of item-label pairs in the context.

**Empirical Validation.** We validate our theoretical results in Figure 6. Unlike our theory, we use a threshold of 0.1 for  $\alpha_3$  and  $\beta_2$ , (rather than 0.5) to better highlight their separation. Training details in Section F.

## 4 Induction Heads in Standard Transformers

### 4.1 Setup

We validate the insights from the previous section and use them to understand standard transformers. We train an autoregressive transformer following the recipe of Vaswani et al. (2017). We train the model using synthetic data to predict the label of a

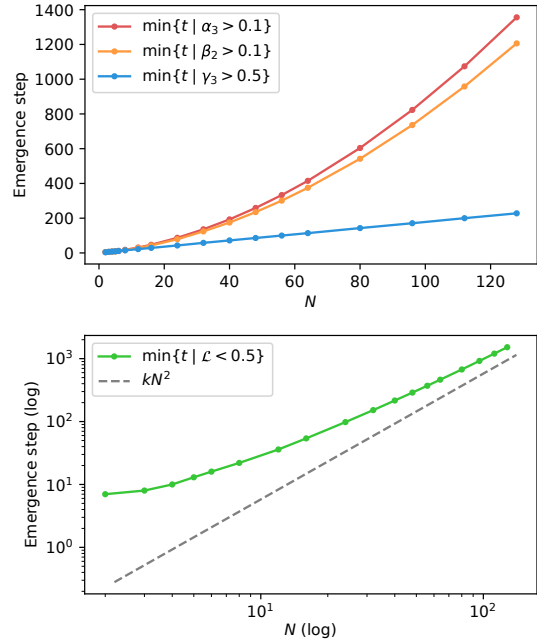


Figure 6: *Top:* The time until the emergence of  $\alpha_3, \beta_2$ , and  $\gamma_3$  for different values of  $N$ . *Bottom:* Time until the emergence of in-context learning (log scale) and its quadratic asymptote.

query item based on the preceding item-label pairs, as depicted in Figure 1. We use only two attention-only layers with one attention head per layer. We remove MLPs from the transformer blocks since they are neither necessary nor useful for the task at hand. We apply a cross-entropy loss only on the query item. We specify the full training details in Section E.

### 4.2 Weight Matrix Structure

**Notation.** We train a transformer with residual stream dimension  $D$ , vocabulary size  $N_T$ , and block size  $N_P$ . We denote the embedding of token  $i$  as  $\mathbf{t}_i \in \mathbb{R}^D$  and the embedding of position  $j$  as  $\mathbf{p}_j \in \mathbb{R}^D$ . We denote the token and positional embedding matrices as  $\mathbf{T} \in \mathbb{R}^{D \times N_T}$  and  $\mathbf{P} \in \mathbb{R}^{D \times N_P}$ , respectively. The layer  $l \in \{1, 2\}$  has the query, key, value, and output matrices  $\mathbf{W}_Q^l, \mathbf{W}_K^l, \mathbf{W}_V^l \in \mathbb{R}^{D_H \times D}$ , and  $\mathbf{W}_O^l \in \mathbb{R}^{D \times D_H}$ , respectively. A final linear output layer  $\mathbf{W}_o \in \mathbb{R}^{N_T \times D}$  is applied. We use  $N_T = N_P = 32$ .

**Architecture.** For an input sequence of length  $L$  with tokens  $\mathbf{X}_T \in \mathbb{R}^{N_T \times L}$  and positions  $\mathbf{X}_P \in \mathbb{R}^{N_P \times L}$  encoded as one-hot vectors, the model will

compute residual streams  $\mathbf{H}_l \in \mathbb{R}^{D \times L}$  as

$$\mathbf{H}_0 = \mathbf{T}\mathbf{X}_T + \mathbf{P}\mathbf{X}_P \quad (17)$$

$$\mathbf{H}_l = \mathbf{H}_{l-1} + \mathbf{W}_O^l \mathbf{W}_V^l \mathbf{H}_{l-1} \sigma(\mathbf{S}_l) \quad (18)$$

$$\mathbf{S}_l = (\mathbf{W}_K^l \mathbf{H}_{l-1})^\top (\mathbf{W}_Q^l \mathbf{H}_{l-1}) \quad (19)$$

where  $l \in \{1, 2\}$  and  $\sigma$  denotes column-wise softmax with causal masking.  $\mathbf{S}_l \in \mathbb{R}^{L \times L}$  is the matrix of attention scores where  $(\mathbf{S}_l)_{i,j}$  denotes the attention score paid by position  $i$  to position  $j$ . The output is computed using a linear layer and softmax  $\mathbf{Y} = \sigma(\mathbf{W}_o \mathbf{H}_2) \in \mathbb{R}^{N_T \times L}$ .

**Explanation.** There are only 4 sub-spaces of the residual stream that are ever activated. First, there is the space spanned by the initial token and positional embeddings,  $\mathbf{t}_i$  and  $\mathbf{p}_j$ . Second, there is the space where the first head writes the retrieved embeddings,  $\mathbf{W}_O^1 \mathbf{W}_V^1 \mathbf{t}_i$  and  $\mathbf{W}_O^1 \mathbf{W}_V^1 \mathbf{p}_j$ . Third, there is the space where the second head writes the retrieved embeddings,  $\mathbf{W}_O^2 \mathbf{W}_V^2 \mathbf{t}_i$  and  $\mathbf{W}_O^2 \mathbf{W}_V^2 \mathbf{p}_j$ . Finally, the second head could retrieve the output of the first head, creating a fourth subspace spanned by  $\mathbf{W}_O^2 \mathbf{W}_V^2 \mathbf{W}_O^1 \mathbf{W}_V^1 \mathbf{t}_i$  and  $\mathbf{W}_O^2 \mathbf{W}_V^2 \mathbf{W}_O^1 \mathbf{W}_V^1 \mathbf{p}_j$ . Since there are  $N_T$  tokens and  $N_P$  positions, each of the four subspaces will have  $N_T + N_P$  dimensions. Moreover, each subspace is highly interpretable, as it can be indexed directly by the corresponding token or position.

**Visualization.** Using these interpretable directions, we can understand the mechanism performed by each layer. For example,  $(\mathbf{W}_K^1 \mathbf{p}_i)^\top \mathbf{W}_Q^1 \mathbf{p}_j$  represents exactly the attention score paid by position  $i$  to position  $j$  during the first layer. In Figure 7, we visualize the key-query matrix products and final output matrix, indexed by these highly interpretable dimensions. Note that this transformation shows how to compute attention scores and outputs for any possible input sequence, and hence Figure 7 is a complete description of the model behavior.

### 4.3 Induction Head Mechanism

In Figure 7, we can see that our weights have a relatively simple and interpretable structure that mirrors the minimal model. Each layer is dominated by a diagonal or subdiagonal within a single block that perfectly aligns the corresponding subspaces. The first layer attends to the previous position. The second layer attends to the token retrieved by the first layer. The final layer outputs the token retrieved by the second layer. This clarifies

the structure of the weight matrices that underlie the induction head mechanism.

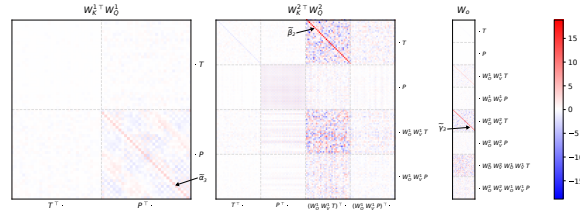


Figure 7: The weights of a two-layer attention-only transformer under our interpretable transformation. Dots  $\cdot$  denote matrix multiplication. For example, the bottom-right block of the left plot,  $\mathbf{P}^\top \mathbf{W}_K^1 \mathbf{W}_Q^1 \mathbf{P}$ , is dominated by the subdiagonal, showing that each position attends to the previous. Some noise is due to random initialization and stochastic gradient descent.

### 4.4 Training Dynamics via Progress Measures

To better understand the emergence of induction heads in standard transformers, we devise three progress measures corresponding exactly to the three relevant structures identified in Figure 7:

$$\tilde{\alpha}_3 = \sum_{i=1}^{N_P} (\mathbf{W}_K^1 \mathbf{p}_{i-1})^\top (\mathbf{W}_Q^1 \mathbf{p}_i) \quad (20)$$

$$\tilde{\beta}_2 = \sum_{i=1}^{N_P} (\mathbf{W}_K^2 \mathbf{W}_O^1 \mathbf{W}_V^1 \mathbf{t}_i)^\top (\mathbf{W}_Q^2 \mathbf{t}_i) \quad (21)$$

$$\tilde{\gamma}_3 = \text{tr}(\mathbf{W}_o \mathbf{W}_O^2 \mathbf{W}_V^2 \mathbf{T}) \quad (22)$$

We train a larger version of the previous transformer and plot the evolution of the progress measures in Figure 8. We observe the same order of emergence as in the minimal formulation: first  $\tilde{\gamma}_3$ , then  $\tilde{\beta}_2$ , and finally  $\tilde{\alpha}_3$ . However, the use of the cross-entropy loss introduces an important difference: achieving low loss requires much larger parameter magnitudes, particularly  $\tilde{\gamma}_3$  and  $\tilde{\beta}_2$ . This results in different post-emergence dynamics and delayed loss reduction.

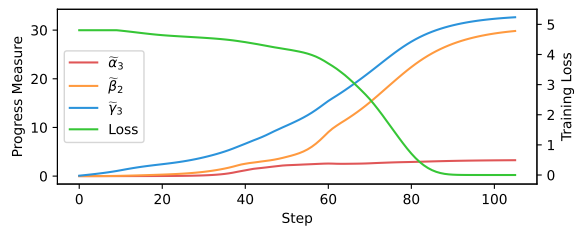


Figure 8: The emergence of induction heads in a standard attention-only transformer, illustrated using progress measures, resembles the disentangled transformer.

## 5 Discussion

### 5.1 How do $\alpha$ , $\beta$ , and $\gamma$ emerge during training?

**The emergence of  $\gamma$ .** Even if  $\alpha$  and  $\beta$  are completely untrained, the attention layers still return something: the average of all items and labels in the context. This average achieves a better loss than predicting zero because it also contains the correct label, and this is exactly what the model learns to predict initially. However, this solution becomes worse when  $N$  is increased. In fact, the gradient towards this solution is inversely proportional to  $N$ , hence why  $\gamma$  emerges in  $\Theta(N)$ .

**The emergence of  $\beta$ .** After the final layer is in place, there is now a gradient for the second layer to attend correctly. Because each label follows immediately after its item, the first layer will always retrieve the item to some extent, even when completely untrained. Taking the causal masking into account, each item will be retrieved the most by its label. This enables the second layer to learn to retrieve based on the query item. However, since the first layer returns a very weak signal (inversely proportional to  $N$ ), the gradient of  $\beta$  will be inversely proportional to  $N^2$ .

**The emergence of  $\alpha$ .** Finally, after  $\beta$  and  $\gamma$  have emerged, there is a very strong gradient for the first layer to attend correctly. This quickly drives the emergence of  $\alpha$ .

### 5.2 The Importance of Context Length

We have established that a longer context length slows down the emergence of induction heads. This fact has interesting implications that are worth exploring in future work.

Chan et al. (2022) have empirically established that the emergence of in-context learning is modulated by data distributional properties specific to natural language, such as burstiness (items appear in clusters rather than being uniformly distributed over time). Our work paves the way for a theoretical understanding of this connection. For example, burstiness could be understood as a modulator of the *effective* context length by reducing the distance between items from the same class. We hypothesize that similar gains could be achieved by other means of reducing the *effective* context length, such as special positional embeddings (Su et al., 2024).

## 6 Related Work

**In-Context Learning** Brown et al. (2020) first observed that LLMs are capable of in-context learning. Chan et al. (2022) empirically showed that the ICL–IWL trade-off is modulated by data distributional properties specific to natural language.

**Induction Heads** Later, Olsson et al. (2022) attributed this ability to a two-layer (Sanford et al., 2024) mechanism (termed *induction head*) that emerges abruptly during training. Crucial to our work, Reddy (2023) proposed a 3-parameter *phenomenological* model of an induction head by directly parameterizing the attention scores. The parameters of this model (denoted as  $\beta_1$ ,  $\alpha$ , and  $\xi$ ) correspond exactly to our three pseudo-parameters ( $\alpha_3$ ,  $\beta_2$ , and  $\gamma_3$ ). Several works (Nichani et al., 2024; Edelman et al., 2024; Chen et al., 2024; Wang et al., 2024a) use a staged training process to show how transformers acquire the ability to learn in-context bigrams. Bietti et al. (2024) study the transformer training dynamics from the perspective of *associative memories*, showing how an induction head can emerge after three steps of gradient descent.

**Mechanistic Interpretability** Several works seek to attribute particular behaviors of neural networks to specific patterns in their weights and activations (Olah et al., 2020; Elhage et al., 2021; Doshi-Velez and Kim, 2017; Olah et al., 2017; Bereska and Gavves, 2024; Cammarata et al., 2020). Friedman et al. (2023) introduce the *disentangled transformer* architecture, which is interpretable by design. Other works focus on multi-step reasoning (Wang et al., 2024b; Muşat, 2025; Cabannes et al., 2024), context-free grammars (Allen-Zhu and Li, 2023), and modular addition (Nanda et al., 2023; Zhong et al., 2023; Gromov, 2023; He et al., 2024).

## 7 Conclusion

In this paper, we have shown how induction heads emerge in an ICL task. Our work paves the way for a better theoretical understanding of transformer learning dynamics. We believe that a similar approach could illuminate other important phenomena in deep learning, such as the *in-context vs. in-weights learning* trade-off, abrupt learning, or the emergence of other transformer circuits.

## 8 Limitations

While our work provides a formal proof for the emergence of induction heads, it relies on several simplifying assumptions.

First, our architectural scope is limited to a disentangled, attention-only transformer. While we empirically show similarities to standard transformers in Section 4, the presence of Layer Normalization, MLPs, and additive residual streams in production-scale models may introduce complex training dynamics not captured by our framework.

Second, our theoretical results assume orthonormal inputs and zero initialization. In practice, token embeddings are not perfectly orthogonal and evolve during training. This may alter the emergence time  $t_{\text{ICL}}$  or the specific sequence of parameter growth.

Finally, our study focuses on a simplified ICL task (exact matching of item-label pairs). Natural language involves varying query positions, semantic nuances, contextual cues, and hierarchical structures. Understanding how the quadratic bound on emergence time translates to data distributions more similar to natural language remains an open question for future work.

## References

- Zeyuan Allen-Zhu and Yuanzhi Li. 2023. Physics of language models: Part 1, learning hierarchical language structures. *arXiv preprint arXiv:2305.13673*.
- Leonard Bereska and Efstratios Gavves. 2024. Mechanistic interpretability for ai safety—a review. *arXiv preprint arXiv:2404.14082*.
- Alberto Bietti, Vivien Cabannes, Diane Bouchacourt, Herve Jegou, and Leon Bottou. 2024. Birth of a transformer: A memory viewpoint. *Advances in Neural Information Processing Systems*, 36.
- Tom Brown, Benjamin Mann, Nick Ryder, Melanie Subbiah, Jared D Kaplan, Prafulla Dhariwal, Arvind Neelakantan, Pranav Shyam, Girish Sastry, Amanda Askell, and 1 others. 2020. Language models are few-shot learners. *Advances in neural information processing systems*, 33:1877–1901.
- Vivien Cabannes, Charles Arnal, Wassim Bouaziz, Xingyu Yang, Francois Charton, and Julia Kempe. 2024. Iteration head: A mechanistic study of chain-of-thought. *Advances in Neural Information Processing Systems*, 37:109101–109122.
- Nick Cammarata, Shan Carter, Gabriel Goh, Chris Olah, Michael Petrov, Ludwig Schubert, Chelsea Voss, Ben Egan, and Swee Kiat Lim. 2020. [Thread: Circuits](https://distill.pub/2020/circuits). *Distill*. <https://distill.pub/2020/circuits>.
- Stephanie Chan, Adam Santoro, Andrew Lampinen, Jane Wang, Aaditya Singh, Pierre Richemond, James McClelland, and Felix Hill. 2022. Data distributional properties drive emergent in-context learning in transformers. *Advances in Neural Information Processing Systems*, 35:18878–18891.
- Siyu Chen, Heejune Sheen, Tianhao Wang, and Zhuoran Yang. 2024. Unveiling induction heads: Provable training dynamics and feature learning in transformers. *arXiv preprint arXiv:2409.10559*.
- Finale Doshi-Velez and Been Kim. 2017. Towards a rigorous science of interpretable machine learning. *arXiv preprint arXiv:1702.08608*.
- Benjamin L Edelman, Ezra Edelman, Surbhi Goel, Eran Malach, and Nikolaos Tsilivis. 2024. The evolution of statistical induction heads: In-context learning markov chains. *arXiv preprint arXiv:2402.11004*.
- Nelson Elhage, Neel Nanda, Catherine Olsson, Tom Henighan, Nicholas Joseph, Ben Mann, Amanda Askell, Yuntao Bai, Anna Chen, Tom Conerly, and 1 others. 2021. A mathematical framework for transformer circuits. *Transformer Circuits Thread*, 1(1):12.
- Dan Friedman, Alexander Wettig, and Danqi Chen. 2023. Learning transformer programs. *Advances in Neural Information Processing Systems*, 36:49044–49067.
- Andrey Gromov. 2023. Grokking modular arithmetic. *arXiv preprint arXiv:2301.02679*.
- Tianyu He, Darshil Doshi, Aritra Das, and Andrey Gromov. 2024. Learning to grok: Emergence of in-context learning and skill composition in modular arithmetic tasks. *Advances in Neural Information Processing Systems*, 37:13244–13273.
- Sepp Hochreiter, A. Steven Younger, and Peter R. Conwell. 2001. Learning to learn using gradient descent. In *Artificial Neural Networks — ICANN 2001*, pages 87–94, Berlin, Heidelberg. Springer Berlin Heidelberg.
- Qian Huang, Eric Zelikman, Sarah Chen, Yuhuai Wu, Gregory Valiant, and Percy S Liang. 2023. Lexinvariant language models. *Advances in Neural Information Processing Systems*, 36:23990–24012.
- Ilya Loshchilov and Frank Hutter. 2017. Decoupled weight decay regularization. *arXiv preprint arXiv:1711.05101*.
- Tiberiu Muşat. 2025. [Mechanism and emergence of stacked attention heads in multi-layer transformers](#). In *The Thirteenth International Conference on Learning Representations*.
- Neel Nanda, Lawrence Chan, Tom Lieberum, Jess Smith, and Jacob Steinhardt. 2023. Progress measures for grokking via mechanistic interpretability. *arXiv preprint arXiv:2301.05217*.

- Eshaan Nichani, Alex Damian, and Jason D Lee. 2024. How transformers learn causal structure with gradient descent. *arXiv preprint arXiv:2402.14735*.
- Chris Olah, Nick Cammarata, Ludwig Schubert, Gabriel Goh, Michael Petrov, and Shan Carter. 2020. Zoom in: An introduction to circuits. *Distill*, 5(3):e00024–001.
- Chris Olah, Alexander Mordvintsev, and Ludwig Schubert. 2017. [Feature visualization](https://distill.pub/2017/feature-visualization). *Distill*. <https://distill.pub/2017/feature-visualization>.
- Catherine Olsson, Nelson Elhage, Neel Nanda, Nicholas Joseph, Nova DasSarma, Tom Henighan, Ben Mann, Amanda Askell, Yuntao Bai, Anna Chen, Tom Conerly, Dawn Drain, Deep Ganguli, Zac Hatfield-Dodds, Danny Hernandez, Scott Johnston, Andy Jones, Jackson Kernion, Liane Lovitt, and 7 others. 2022. In-context learning and induction heads. *Transformer Circuits Thread*. <https://transformer-circuits.pub/2022/in-context-learning-and-induction-heads/index.html>.
- Gautam Reddy. 2023. The mechanistic basis of data dependence and abrupt learning in an in-context classification task. In *The Twelfth International Conference on Learning Representations*.
- Clayton Sanford, Daniel Hsu, and Matus Telgarsky. 2024. One-layer transformers fail to solve the induction heads task. *arXiv preprint arXiv:2408.14332*.
- Jianlin Su, Murtadha Ahmed, Yu Lu, Shengfeng Pan, Wen Bo, and Yunfeng Liu. 2024. [Roformer: Enhanced transformer with rotary position embedding](#). *Neurocomputing*, 568:127063.
- Ashish Vaswani, Noam Shazeer, Niki Parmar, Jakob Uszkoreit, Llion Jones, Aidan N Gomez, Łukasz Kaiser, and Illia Polosukhin. 2017. Attention is all you need. *Advances in neural information processing systems*, 30.
- Mingze Wang, Ruoxi Yu, Lei Wu, and 1 others. 2024a. How transformers implement induction heads: Approximation and optimization analysis. *arXiv preprint arXiv:2410.11474*.
- Zhiwei Wang, Yunji Wang, Zhongwang Zhang, Zhangchen Zhou, Hui Jin, Tianyang Hu, Jiacheng Sun, Zhenguo Li, Yaoyu Zhang, and Zhi-Qin John Xu. 2024b. The buffer mechanism for multi-step information reasoning in language models. *arXiv preprint arXiv:2405.15302*.
- Ziqian Zhong, Ziming Liu, Max Tegmark, and Jacob Andreas. 2023. The clock and the pizza: Two stories in mechanistic explanation of neural networks. *Advances in neural information processing systems*, 36:27223–27250.

## A Weights Structure Full Proof for Theorem 1

### A.1 Summary

Our strategy is to show that if  $W^{(1)}$ ,  $W^{(2)}$ , and  $W^{(3)}$  have this structure, then their gradients also have the same structure. Since we start from zero initialization, by induction, this means that the structure is preserved throughout the entire training process.

To prove the structure of the gradient, we apply a carefully chosen rotation to the entire data distribution. Since the data distribution is isotropic, the rotation will not change the data distribution, so the expected gradient will also remain unchanged.

However, we are also able to show that our rotation induces a specific similarity transformation of the gradient:

$$\mathbb{E} \left[ \frac{\partial \mathcal{L}}{\partial \mathbf{W}_{ij}^{(k)}} \right] = F \mathbb{E} \left[ \frac{\partial \mathcal{L}}{\partial \mathbf{W}_{ij}^{(k)}} \right] F^\top$$

where  $F$  is an orthogonal or block-orthogonal matrix and  $\mathbf{W}_{ij}^{(k)}$  is a block of a weight matrix. From this we are able to show that the expected gradient must have the desired structure.

### A.2 Prerequisites

#### A.2.1 Orthogonal Transformations

**Definition 4. Orthogonal Matrix.** We say that a matrix  $E \in \mathbb{R}^{k \times k}$  is orthogonal if it satisfies  $EE^\top = E^\top E = I$ .

**Proposition 1.** Let  $A \in \mathbb{R}^{k \times k}$  be some matrix. If  $EAE^\top = A$  holds **for all** orthogonal matrices  $E \in \mathbb{R}^{k \times k}$ , then it follows that  $A = \alpha I$  for some  $\alpha \in \mathbb{R}$ .

*Proof. Step 1. All off-diagonal entries of  $A$  vanish.*

Fix an index  $j \in \{1, \dots, k\}$  and let

$$E = \text{diag}(1, \dots, 1, -1, 1, \dots, 1)$$

be the diagonal orthogonal matrix with entry  $-1$  in the  $j$ th position and  $+1$  elsewhere. Then

$$(EAE^\top)_{i\ell} = E_{ii} A_{i\ell} E_{\ell\ell} = \begin{cases} A_{i\ell}, & i, \ell \neq j, \\ -A_{i\ell}, & \text{exactly one of } i, \ell = j, \\ A_{jj}, & i = \ell = j. \end{cases}$$

Since  $EAE^\top = A$ , it follows that  $-A_{ij} = A_{ij}$  for every  $i \neq j$ , whence  $A_{ij} = 0$ . Varying  $j$  shows all off-diagonal entries vanish, so

$$A = \text{diag}(a_{11}, a_{22}, \dots, a_{kk}).$$

*Step 2. All diagonal entries of  $A$  coincide.*

Let  $E$  be any permutation matrix which swaps two coordinates  $i$  and  $j$ . Then  $E$  is orthogonal and

$$EAE^\top = \text{diag}(\dots, a_{jj}, \dots, a_{ii}, \dots),$$

interchanging the  $i$ th and  $j$ th diagonal entries of  $A$ . By invariance  $EAE^\top = A$ , so  $a_{ii} = a_{jj}$ . Since  $i, j$  were arbitrary, there exists  $\alpha \in \mathbb{R}$  such that

$$a_{11} = a_{22} = \dots = a_{kk} = \alpha,$$

and hence  $A = \alpha I$ .

□

## A.2.2 Block-Orthogonal Transformations

**Definition 5. Block-Orthogonal Matrix.** We say that a matrix  $F \in \mathbb{R}^{2k \times 2k}$  is block-orthogonal if it has either of the following two forms:

$$F = \left[ \begin{array}{c|c} E & \mathbf{0} \\ \hline \mathbf{0} & E \end{array} \right] \quad \text{or} \quad F = \left[ \begin{array}{c|c} \mathbf{0} & E \\ \hline E & \mathbf{0} \end{array} \right]$$

where  $E \in \mathbb{R}^{k \times k}$  is an orthogonal matrix.

**Proposition 2.** Let  $A \in \mathbb{R}^{2k \times 2k}$  be some matrix. If  $F A F^\top = A$  holds for all block-orthogonal matrices  $F \in \mathbb{R}^{2k \times 2k}$ , then it follows that

$$A = \left[ \begin{array}{c|c} \alpha I & \beta I \\ \hline \beta I & \alpha I \end{array} \right]$$

for some  $\alpha, \beta \in \mathbb{R}$ .

**Remark 1.** Note that this condition is weaker than the condition stated in Proposition 1, since not all orthogonal matrices are also block-orthogonal. Hence, the condition in Proposition 2 guarantees a structure that is less specific than Proposition 1.

*Proof.* We write

$$A = \left[ \begin{array}{c|c} A_{11} & A_{12} \\ \hline A_{21} & A_{22} \end{array} \right],$$

where each block  $A_{ij} \in \mathbb{R}^{k \times k}$ .

*Step 1.* All blocks are scalar matrices.

For any orthogonal matrix  $E$ , we can set

$$F = \left[ \begin{array}{c|c} E & \mathbf{0} \\ \hline \mathbf{0} & E \end{array} \right].$$

Then

$$F A F^\top = \left[ \begin{array}{c|c} EA_{11}E^\top & EA_{12}E^\top \\ \hline EA_{21}E^\top & EA_{22}E^\top \end{array} \right] = \left[ \begin{array}{c|c} A_{11} & A_{12} \\ \hline A_{21} & A_{22} \end{array} \right] = A,$$

so  $E A_{ij} E^\top = A_{ij}$  for all  $i, j$ . By the previous proposition each block is a scalar multiple of the identity,  $A_{ij} = \alpha_{ij} I_k$ , for some  $\alpha_{ij} \in \mathbb{R}$ . Therefore,

$$A = \left[ \begin{array}{c|c} \alpha_{11} I & \alpha_{12} I \\ \hline \alpha_{21} I & \alpha_{22} I \end{array} \right].$$

*Step 2.* Diagonally opposed blocks coincide. By setting

$$F = \left[ \begin{array}{c|c} \mathbf{0} & I \\ \hline I & \mathbf{0} \end{array} \right]$$

we obtain

$$F A F^\top = \left[ \begin{array}{c|c} A_{22} & A_{21} \\ \hline A_{12} & A_{11} \end{array} \right]$$

which yields  $\alpha_{11} = \alpha_{22}$ ,  $\alpha_{12} = \alpha_{21}$ . By writing  $\alpha = \alpha_{11}$  and  $\beta = \alpha_{12}$ , we obtain

$$A = \left[ \begin{array}{c|c} \alpha I & \beta I \\ \hline \beta I & \alpha I \end{array} \right]$$

□

### A.2.3 Combined Transformations

**Proposition 3.** Let  $A \in \mathbb{R}^{2k \times 2k}$  be some matrix. If  $EAF = A$  holds for all orthogonal matrices  $E$  and block-orthogonal matrices  $F$ , then  $A = \mathbf{0}$ .

*Proof.* By setting  $E = I$  and  $F = -I$ , we get  $A = -A$ . Therefore,  $A = \mathbf{0}$ .  $\square$

### A.2.4 Block-Swap Transformation

**Definition 6. Block-Swap Matrix.** We say that a matrix  $M \in \mathbb{R}^{2k \times 2k}$  is block-swap if it has the following form:

$$M = \left[ \begin{array}{c|c} \mathbf{0} & I \\ \hline I & \mathbf{0} \end{array} \right]$$

where  $I \in \mathbb{R}^{k \times k}$  is the identity matrix.

**Proposition 4.** If  $M \in \mathbb{R}^{2k \times 2k}$  is a block-swap matrix and  $F \in \mathbb{R}^{2k \times 2k}$  is a block-orthogonal matrix, then  $FMF^\top = M$ .

*Proof. Case 1. The orthogonal blocks of  $F$  are on the main diagonal.*

Assume that

$$F = \left[ \begin{array}{c|c} E & \mathbf{0} \\ \hline \mathbf{0} & E \end{array} \right]$$

Then,

$$\begin{aligned} FMF^\top &= \left[ \begin{array}{c|c} E & \mathbf{0} \\ \hline \mathbf{0} & E \end{array} \right] \left[ \begin{array}{c|c} \mathbf{0} & I \\ \hline I & \mathbf{0} \end{array} \right] \left[ \begin{array}{c|c} E^\top & \mathbf{0} \\ \hline \mathbf{0} & E^\top \end{array} \right] \\ &= \left[ \begin{array}{c|c} \mathbf{0} & E \\ \hline E & \mathbf{0} \end{array} \right] \left[ \begin{array}{c|c} E^\top & \mathbf{0} \\ \hline \mathbf{0} & E^\top \end{array} \right] \\ &= \left[ \begin{array}{c|c} \mathbf{0} & I \\ \hline I & \mathbf{0} \end{array} \right] \end{aligned}$$

*Case 2. The orthogonal blocks of  $F$  are on the secondary diagonal.*

Assume that

$$F = \left[ \begin{array}{c|c} \mathbf{0} & E \\ \hline E & \mathbf{0} \end{array} \right]$$

Then,

$$\begin{aligned} FMF^\top &= \left[ \begin{array}{c|c} \mathbf{0} & E \\ \hline E & \mathbf{0} \end{array} \right] \left[ \begin{array}{c|c} \mathbf{0} & I \\ \hline I & \mathbf{0} \end{array} \right] \left[ \begin{array}{c|c} \mathbf{0} & E^\top \\ \hline E^\top & \mathbf{0} \end{array} \right] \\ &= \left[ \begin{array}{c|c} E & \mathbf{0} \\ \hline \mathbf{0} & E \end{array} \right] \left[ \begin{array}{c|c} \mathbf{0} & E^\top \\ \hline E^\top & \mathbf{0} \end{array} \right] \\ &= \left[ \begin{array}{c|c} \mathbf{0} & I \\ \hline I & \mathbf{0} \end{array} \right] \end{aligned}$$

$\square$

## A.3 Setup

Recall the architecture and loss:

$$U = \left[ X \mid \sigma(XW^{(1)}X^\top)X \right] \quad V = \left[ U \mid \sigma(UW^{(2)}U^\top)U \right]$$

$$z = V_{2N+1}W^{(3)} \quad \mathcal{L} = \|y - z\|^2$$

where  $\sigma$  denotes the softmax function with causal masking,  $[\cdot | \cdot]$  denotes matrix concatenation, and

$$\begin{aligned} W^{(1)} &\in \mathbb{R}^{2D \times 2D} & W^{(2)} &\in \mathbb{R}^{4D \times 4D} & W^{(3)} &\in \mathbb{R}^{8D \times D} \\ U &\in \mathbb{R}^{(2N+1) \times 4D} & V &\in \mathbb{R}^{(2N+1) \times 8D} & z &\in \mathbb{R}^D \\ X &\in \mathbb{R}^{(2N+1) \times 2D} & y &\in \mathbb{R}^D \end{aligned}$$

The data is generated as:

$$\begin{aligned} X_{2i-1} &= [a_i | p_i] & X_{2i} &= [b_i | p_i M] & \forall i &\in \{1, \dots, N\} \\ X_{2N+1} &= [a_q | 0] & y &= b_q \end{aligned}$$

where

$$a_i, b_i, p_i \in \mathbb{R}^D \quad q \in \{1, 2, \dots, N\} \quad M = \begin{bmatrix} \mathbf{0} & I \\ I & \mathbf{0} \end{bmatrix}$$

All vectors are treated as **row vectors**.

#### A.4 Additional Notation

We introduce

$$\begin{aligned} S &= X \mathbf{W}^{(1)} X^\top & T &= \sigma(S) \\ P &= U \mathbf{W}^{(2)} U^\top & Q &= \sigma(P) \end{aligned}$$

where  $S, T, P, Q \in \mathbb{R}^{(2N+1) \times (2N+1)}$ . This gives

$$U = [X | TX] \quad V = [U | QU]$$

We also introduce notation for all blocks of size  $D$ :

$$\begin{aligned} X &= [X_1 \quad X_2] & U &= [U_1 \quad U_2 \quad U_3 \quad U_4] \\ V &= [V_1 \quad V_2 \quad V_3 \quad V_4 \quad V_5 \quad V_6 \quad V_7 \quad V_8] \\ \mathbf{W}^{(1)} &= \begin{bmatrix} \mathbf{W}_{11}^{(1)} & \mathbf{W}_{12}^{(1)} \\ \mathbf{W}_{21}^{(1)} & \mathbf{W}_{22}^{(1)} \end{bmatrix} & \mathbf{W}^{(2)} &= \begin{bmatrix} \mathbf{W}_{11}^{(2)} & \mathbf{W}_{12}^{(2)} & \mathbf{W}_{13}^{(2)} & \mathbf{W}_{14}^{(2)} \\ \mathbf{W}_{11}^{(2)} & \mathbf{W}_{12}^{(2)} & \mathbf{W}_{13}^{(2)} & \mathbf{W}_{14}^{(2)} \\ \mathbf{W}_{11}^{(2)} & \mathbf{W}_{12}^{(2)} & \mathbf{W}_{13}^{(2)} & \mathbf{W}_{14}^{(2)} \\ \mathbf{W}_{11}^{(2)} & \mathbf{W}_{12}^{(2)} & \mathbf{W}_{13}^{(2)} & \mathbf{W}_{14}^{(2)} \end{bmatrix} \\ \mathbf{W}^{(3)} &= [\mathbf{W}_1^{(3)} \quad \mathbf{W}_2^{(3)} \quad \mathbf{W}_3^{(3)} \quad \mathbf{W}_4^{(3)} \quad \mathbf{W}_5^{(3)} \quad \mathbf{W}_6^{(3)} \quad \mathbf{W}_7^{(3)} \quad \mathbf{W}_8^{(3)}] \end{aligned}$$

#### A.5 Data Rotations

We apply an orthogonal transformation  $E$  to the items and labels, and a block-orthogonal transformation  $F$  to the positional embeddings:

$$a'_i = a_i E \quad b'_i = b_i E \quad p'_i = p_i F \quad \forall i \in \{1, \dots, N\}$$

where  $E$  and  $F$  satisfy Definitions 4 and 5, respectively. We refer to the new variables as  $X', y', U', V', z'$ , and  $\mathcal{L}'$ .

Since the data is isotropic, we have that  $\mathbb{E}[\mathcal{L}] = \mathbb{E}[\mathcal{L}']$ . By the linearity of expectation and differentiation, we obtain

$$\mathbb{E} \left[ \frac{\partial \mathcal{L}}{\partial \mathbf{W}^{(k)}} \right] = \mathbb{E} \left[ \frac{\partial \mathcal{L}'}{\partial \mathbf{W}^{(k)}} \right]$$

This also holds for all sub-blocks of  $\mathbf{W}^{(1)}$ ,  $\mathbf{W}^{(2)}$ , and  $\mathbf{W}^{(3)}$ ,

$$\mathbb{E} \left[ \frac{\partial \mathcal{L}}{\partial \mathbf{W}_{ij}^{(k)}} \right] = \mathbb{E} \left[ \frac{\partial \mathcal{L}'}{\partial \mathbf{W}_{ij}^{(k)}} \right]$$

However, as we show below, our rotation induces specific transformations of the gradient blocks. Using Propositions 1 to 3, we are able to show that each gradient block has the desired structure.

Specifically, for each gradient block, we will show that one of the following four conditions holds for all  $E$  and  $F$ , implying the desired structure:

$$\begin{aligned} \mathbb{E} \left[ \frac{\partial \mathcal{L}'}{\partial \mathbf{W}_{ij}^{(k)}} \right] = E \mathbb{E} \left[ \frac{\partial \mathcal{L}'}{\partial \mathbf{W}_{ij}^{(k)}} \right] E^\top &\implies \mathbb{E} \left[ \frac{\partial \mathcal{L}}{\partial \mathbf{W}_{ij}^{(k)}} \right] = \alpha I \\ \mathbb{E} \left[ \frac{\partial \mathcal{L}'}{\partial \mathbf{W}_{ij}^{(k)}} \right] = F \mathbb{E} \left[ \frac{\partial \mathcal{L}'}{\partial \mathbf{W}_{ij}^{(k)}} \right] F^\top &\implies \mathbb{E} \left[ \frac{\partial \mathcal{L}}{\partial \mathbf{W}_{ij}^{(k)}} \right] = \begin{bmatrix} \alpha I & \beta I \\ \beta I & \alpha I \end{bmatrix} \\ \mathbb{E} \left[ \frac{\partial \mathcal{L}'}{\partial \mathbf{W}_{ij}^{(k)}} \right] = E \mathbb{E} \left[ \frac{\partial \mathcal{L}'}{\partial \mathbf{W}_{ij}^{(k)}} \right] F^\top &\implies \mathbb{E} \left[ \frac{\partial \mathcal{L}}{\partial \mathbf{W}_{ij}^{(k)}} \right] = \mathbf{0} \\ \mathbb{E} \left[ \frac{\partial \mathcal{L}'}{\partial \mathbf{W}_{ij}^{(k)}} \right] = F \mathbb{E} \left[ \frac{\partial \mathcal{L}'}{\partial \mathbf{W}_{ij}^{(k)}} \right] E^\top &\implies \mathbb{E} \left[ \frac{\partial \mathcal{L}}{\partial \mathbf{W}_{ij}^{(k)}} \right] = \mathbf{0} \end{aligned}$$

## A.6 Forward Pass

We will now observe how our rotation changes the intermediate and final results of our model.

First, note the rotated inputs and outputs:

$$X'_1 = X_1 E \quad X'_2 = X_2 F \quad y' = y E$$

Recall that we are assuming that  $\mathbf{W}^{(1)}$ ,  $\mathbf{W}^{(2)}$ , and  $\mathbf{W}^{(3)}$  already have the desired structure, with the goal to prove that the gradient has the same structure:

$$\begin{aligned} W^{(1)} &= \left[ \begin{array}{c|c} \alpha_1 I & \mathbf{0} \\ \mathbf{0} & \alpha_2 I + \alpha_3 M \end{array} \right] \\ W^{(2)} &= \left[ \begin{array}{c|c|c|c} \beta_1 I & \mathbf{0} & \beta_2 I & \mathbf{0} \\ \mathbf{0} & \beta_3 I + \beta_4 M & \mathbf{0} & \beta_5 I + \beta_6 M \\ \beta_7 I & \mathbf{0} & \beta_8 I & \mathbf{0} \\ \mathbf{0} & \beta_9 I + \beta_{10} M & \mathbf{0} & \beta_{11} I + \beta_{12} M \end{array} \right] \\ W^{(3)} &= [ \gamma_1 I \mid \mathbf{0} \mid \gamma_2 I \mid \mathbf{0} \mid \gamma_3 I \mid \mathbf{0} \mid \gamma_4 I \mid \mathbf{0} ] \end{aligned}$$

### A.6.1 First Layer

The first attention layer gives:

$$\begin{aligned}
S &= X\mathbf{W}^{(1)}X^\top \\
&= X_1\mathbf{W}_{11}^{(1)}X_1^\top + X_1\mathbf{W}_{12}^{(1)}X_2^\top + X_2\mathbf{W}_{21}^{(1)}X_1^\top + X_2\mathbf{W}_{22}^{(1)}X_2^\top \\
&= \alpha_1X_1X_1^\top + \alpha_2X_2X_2^\top + \alpha_3X_2MX_2^\top \\
S' &= X'\mathbf{W}^{(1)}X'^\top \\
&= X'_1\mathbf{W}_{11}^{(1)}X_1'^\top + X'_1\mathbf{W}_{12}^{(1)}X_2'^\top + X'_2\mathbf{W}_{21}^{(1)}X_1'^\top + X'_2\mathbf{W}_{22}^{(1)}X_2'^\top \\
&= \alpha_1X'_1X_1'^\top + \alpha_2X'_2X_2'^\top + \alpha_3X'_2MX_2'^\top \\
&= \alpha_1X_1EE^\top X_1^\top + \alpha_2X_2FF^\top X_2^\top + \alpha_3X_2FMF^\top X_2^\top \\
&= \alpha_1X_1X_1^\top + \alpha_2X_2X_2^\top + \alpha_3X_2MX_2^\top
\end{aligned}$$

Therefore,  $S' = S$  and  $T' = T = \sigma(S)$ . This gives us:

$$U'_1 = U_1E \quad U'_2 = U_2F \quad U'_3 = U_3E \quad U'_4 = U_4F$$

### A.6.2 Second Layer

The second attention layer gives:

$$\begin{aligned}
P &= U\mathbf{W}^{(2)}U^\top \\
&= \sum U_i\mathbf{W}_{ij}^{(2)}U_j^\top \\
&= \beta_1U_1U_1^\top + \beta_2U_1U_3^\top + \beta_7U_3U_1^\top + \beta_8U_3U_3^\top \\
&\quad + \beta_3U_2U_2^\top + \beta_5U_2U_4^\top + \beta_9U_4U_2^\top + \beta_{11}U_4U_4^\top \\
&\quad + \beta_4U_2MU_2^\top + \beta_6U_2MU_4^\top + \beta_{10}U_4MU_2^\top + \beta_{12}U_4MU_4^\top \\
P' &= U'\mathbf{W}^{(2)}U'^\top \\
&= \sum U'_i\mathbf{W}_{ij}^{(2)}U_j'^\top \\
&= \beta_1U'_1U_1'^\top + \beta_2U'_1U_3'^\top + \beta_7U'_3U_1'^\top + \beta_8U'_3U_3'^\top \\
&\quad + \beta_3U'_2U_2'^\top + \beta_5U'_2U_4'^\top + \beta_9U'_4U_2'^\top + \beta_{11}U'_4U_4'^\top \\
&\quad + \beta_4U'_2MU_2'^\top + \beta_6U'_2MU_4'^\top + \beta_{10}U'_4MU_2'^\top + \beta_{12}U'_4MU_4'^\top \\
&= \beta_1U_1EE^\top U_1^\top + \beta_2U_1EE^\top U_3^\top + \beta_7U_3EE^\top U_1^\top + \beta_8U_3EE^\top U_3^\top \\
&\quad + \beta_3U_2FF^\top U_2^\top + \beta_5U_2FF^\top U_4^\top + \beta_9U_4FF^\top U_2^\top + \beta_{11}U_4FF^\top U_4^\top \\
&\quad + \beta_4U_2FMF^\top U_2^\top + \beta_6U_2FMF^\top U_4^\top + \beta_{10}U_4FMF^\top U_2^\top + \beta_{12}U_4FMF^\top U_4^\top \\
&= \beta_1U_1U_1^\top + \beta_2U_1U_3^\top + \beta_7U_3U_1^\top + \beta_8U_3U_3^\top \\
&\quad + \beta_3U_2U_2^\top + \beta_5U_2U_4^\top + \beta_9U_4U_2^\top + \beta_{11}U_4U_4^\top \\
&\quad + \beta_4U_2MU_2^\top + \beta_6U_2MU_4^\top + \beta_{10}U_4MU_2^\top + \beta_{12}U_4MU_4^\top
\end{aligned}$$

Therefore,  $P' = P$  and  $Q' = Q = \sigma(P)$ . This gives us:

$$\begin{aligned}
V'_1 &= V_1E & V'_2 &= V_2F & V'_3 &= V_3E & V'_4 &= V_4F \\
V'_5 &= V_5E & V'_6 &= V_6F & V'_7 &= V_7E & V'_8 &= V_8F
\end{aligned}$$

### A.6.3 Output Layer

Finally, the output layer gives:

$$\begin{aligned}
z &= V_{2N+1} \mathbf{W}^{(3)} \\
&= \sum (V_i)_{2N+1} \mathbf{W}_i^{(3)} \\
&= \gamma_1 (V_1)_{2N+1} + \gamma_2 (V_3)_{2N+1} + \gamma_3 (V_5)_{2N+1} + \gamma_4 (V_7)_{2N+1} \\
z' &= V'_{2N+1} \mathbf{W}^{(3)} \\
&= \sum (V'_i)_{2N+1} \mathbf{W}_i^{(3)} \\
&= \gamma_1 (V'_1)_{2N+1} + \gamma_2 (V'_3)_{2N+1} + \gamma_3 (V'_5)_{2N+1} + \gamma_4 (V'_7)_{2N+1} \\
&= \gamma_1 (V_1)_{2N+1} E + \gamma_2 (V_3)_{2N+1} E + \gamma_3 (V_5)_{2N+1} E + \gamma_4 (V_7)_{2N+1} E \\
&= zE
\end{aligned}$$

## A.7 Backward Pass

We now show how the rotation transforms the gradient of each weight block.

### A.7.1 Output Layer

$$\begin{aligned}
\frac{\partial \mathcal{L}}{\partial z} &= 2(z - y) \\
\frac{\partial \mathcal{L}'}{\partial z'} &= 2(z' - y') = 2(zE - yE) = 2(z - y)E = \frac{\partial \mathcal{L}}{\partial z} E \\
\frac{\partial \mathcal{L}}{\partial \mathbf{W}_i^{(3)}} &= ((V_i)_{2N+1})^\top \left( \frac{\partial \mathcal{L}}{\partial z} \right) \\
\frac{\partial \mathcal{L}'}{\partial \mathbf{W}_i^{(3)}} &= ((V'_i)_{2N+1})^\top \left( \frac{\partial \mathcal{L}'}{\partial z'} \right)
\end{aligned}$$

**Scalar Blocks.** For all  $i \in \{1, 3, 5, 7\}$ , we get

$$\begin{aligned}
\frac{\partial \mathcal{L}'}{\partial \mathbf{W}_i^{(3)}} &= ((V'_i)_{2N+1})^\top \left( \frac{\partial \mathcal{L}'}{\partial z'} \right) \\
&= E^\top ((V_i)_{2N+1})^\top \left( \frac{\partial \mathcal{L}}{\partial z} \right) E \\
&= E^\top \frac{\partial \mathcal{L}}{\partial \mathbf{W}_i^{(3)}} E
\end{aligned}$$

Taking the expectation over the entire data distribution, we obtain that the following holds for any orthogonal transformation  $E$ :

$$\mathbb{E} \left[ \frac{\partial \mathcal{L}}{\partial \mathbf{W}_i^{(3)}} \right] = \mathbb{E} \left[ \frac{\partial \mathcal{L}'}{\partial \mathbf{W}_i^{(3)}} \right] = \mathbb{E} \left[ E^\top \frac{\partial \mathcal{L}'}{\partial \mathbf{W}_i^{(3)}} E \right] = E^\top \mathbb{E} \left[ \frac{\partial \mathcal{L}}{\partial \mathbf{W}_i^{(3)}} \right] E$$

Applying Proposition 1, we get that

$$\mathbb{E} \left[ \frac{\partial \mathcal{L}}{\partial \mathbf{W}_i^{(3)}} \right] = \alpha I$$

**Zero Blocks.** For all  $i \in \{2, 4, 6, 8\}$ , we get

$$\begin{aligned}\frac{\partial \mathcal{L}'}{\partial \mathbf{W}_i^{(3)}} &= \left( (V'_i)_{2N+1} \right)^\top \left( \frac{\partial \mathcal{L}'}{\partial z'} \right) \\ &= F^\top \left( (V_i)_{2N+1} \right)^\top \left( \frac{\partial \mathcal{L}}{\partial z} \right) E \\ &= F^\top \frac{\partial \mathcal{L}}{\partial \mathbf{W}_i^{(3)}} E\end{aligned}$$

Taking the expectation over the entire data distribution, we obtain that the following holds for any  $E$  and  $F$ :

$$\mathbb{E} \left[ \frac{\partial \mathcal{L}}{\partial \mathbf{W}_i^{(3)}} \right] = F^\top \mathbb{E} \left[ \frac{\partial \mathcal{L}}{\partial \mathbf{W}_i^{(3)}} \right] E$$

Applying Proposition 3, we get that

$$\mathbb{E} \left[ \frac{\partial \mathcal{L}}{\partial \mathbf{W}_i^{(3)}} \right] = \mathbf{0}$$

**Gradient Propagation** Applying the chain rule, we get

$$\frac{\partial \mathcal{L}}{\partial V_{2N+1}} = \frac{\partial \mathcal{L}}{\partial z} \frac{\partial z}{\partial V_{2N+1}} = 2(z - y) \mathbf{W}^{(3)\top}$$

For all  $i \in \{1, 3, 5, 7\}$ , we get

$$\frac{\partial \mathcal{L}'}{\partial (V'_i)_{2N+1}} = 2(z' - y') \mathbf{W}_i^{(3)\top} = 2(z - y) E \mathbf{W}_i^{(3)\top} = \frac{\partial \mathcal{L}}{\partial (V_i)_{2N+1}} E$$

For all  $i \in \{2, 4, 6, 8\}$ , we get

$$\frac{\partial \mathcal{L}}{\partial (V_i)_{2N+1}} = 2(z - y) \mathbf{W}_i^{(3)} = \mathbf{0}$$

For all  $i \in \{1, \dots, 8\}$  and  $j \leq 2N$ , we get

$$\frac{\partial \mathcal{L}}{\partial (V_i)_j} = \frac{\partial \mathcal{L}}{\partial (V'_i)_j} = \mathbf{0}$$

Putting everything together, the following holds for all  $j \leq 2N + 1$

$$\frac{\partial \mathcal{L}}{\partial (V_i)_j} = \frac{\partial \mathcal{L}'}{\partial (V'_i)_j} E \quad \text{if } i \in \{1, 3, 5, 7\} \quad (23)$$

$$\frac{\partial \mathcal{L}}{\partial (V_i)_j} = \frac{\partial \mathcal{L}'}{\partial (V'_i)_j} = \mathbf{0} \quad \text{if } i \in \{2, 4, 6, 8\} \quad (24)$$

## A.7.2 Second Layer

Since  $V = [U \mid QU]$ , we have that

$$\frac{\partial (V_i)_j}{\partial Q_{jk}} = \begin{cases} U_{i-4} & i > 4 \\ \mathbf{0} & i \leq 4 \end{cases}$$

Therefore,

$$\frac{\partial \mathcal{L}'}{\partial (V'_i)_j} \frac{\partial (V'_i)_j}{\partial Q'_{jk}} = \frac{\partial \mathcal{L}}{\partial (V_i)_j} E^\top E \frac{\partial (V_i)_j}{\partial Q_{jk}} = \frac{\partial \mathcal{L}}{\partial (V_i)_j} \frac{\partial (V_i)_j}{\partial Q_{jk}} \quad i \in \{5, 7\}$$

$$\frac{\partial \mathcal{L}'}{\partial (V'_i)_j} \frac{\partial (V'_i)_j}{\partial Q'_{jk}} = \frac{\partial \mathcal{L}}{\partial (V_i)_j} \frac{\partial (V_i)_j}{\partial Q_{jk}} = \mathbf{0} \quad i \notin \{5, 7\}$$

Additionally, since  $P' = P$  and  $Q' = Q$ , we have that

$$\frac{\partial Q'_{jk}}{\partial P'_{jl}} = \frac{\partial Q_{jk}}{\partial P_{jl}}$$

This gives us

$$\begin{aligned} \frac{\partial \mathcal{L}'}{\partial P'_{kl}} &= \sum_{ij} \frac{\partial \mathcal{L}'}{\partial (V'_i)_j} \frac{\partial (V'_i)_j}{\partial Q'_{kj}} \frac{\partial Q'_{kj}}{\partial P'_{kl}} \\ &= \sum_{ij} \frac{\partial \mathcal{L}}{\partial (V_i)_k} \frac{\partial (V_i)_k}{\partial Q_{kj}} \frac{\partial Q_{kj}}{\partial P_{kl}} \\ &= \frac{\partial \mathcal{L}}{\partial P_{kl}} \end{aligned}$$

Additionally,

$$\frac{\partial \mathcal{L}}{\partial \mathbf{W}_{ij}^{(2)}} = \sum_{kl} \frac{\partial \mathcal{L}}{\partial P_{kl}} \frac{\partial P_{kl}}{\partial \mathbf{W}_{ij}^{(2)}} = \sum_{kl} \frac{\partial \mathcal{L}}{\partial P_{kl}} (U_i)_k^\top (U_j)_l$$

which gives us the transformed gradient:

$$\begin{aligned} \frac{\partial \mathcal{L}'}{\partial \mathbf{W}_{ij}^{(2)}} &= \sum_{kl} \frac{\partial \mathcal{L}'}{\partial P'_{kl}} \frac{\partial P'_{kl}}{\partial \mathbf{W}_{ij}^{(2)}} = \sum_{kl} \frac{\partial \mathcal{L}}{\partial P_{kl}} (U'_i)_k^\top (U'_j)_l \\ &= \begin{cases} E^\top \frac{\partial \mathcal{L}}{\partial \mathbf{W}_{ij}^{(2)}} E & \text{if } i \text{ odd, } j \text{ odd} \\ E^\top \frac{\partial \mathcal{L}}{\partial \mathbf{W}_{ij}^{(2)}} F & \text{if } i \text{ odd, } j \text{ even} \\ F^\top \frac{\partial \mathcal{L}}{\partial \mathbf{W}_{ij}^{(2)}} E & \text{if } i \text{ even, } j \text{ odd} \\ F^\top \frac{\partial \mathcal{L}}{\partial \mathbf{W}_{ij}^{(2)}} F & \text{if } i \text{ even, } j \text{ even} \end{cases} \end{aligned}$$

The desired structure follows from computing the expected gradient over the entire distribution and applying Propositions 1 to 3.

### Gradient Propagation

Applying the chain rule, we get

$$\frac{\partial \mathcal{L}'}{\partial (U'_i)_j} = \frac{\partial \mathcal{L}'}{\partial (V'_i)_j} + Q'^\top \frac{\partial \mathcal{L}'}{\partial (V'_{i+4})_j} + \sum_k \frac{\partial \mathcal{L}'}{\partial P'_{jk}} \frac{\partial P'_{jk}}{\partial (U'_i)_j} \quad (25)$$

We also have that

$$\frac{\partial P_{jk}}{\partial (U_i)_j} = (U_i)_k \quad \frac{\partial P'_{jk}}{\partial (U'_i)_j} = (U'_i)_k = \begin{cases} (U_i)_k E & \text{if } i \text{ odd} \\ (U_i)_k F & \text{if } i \text{ even} \end{cases} \quad (26)$$

Combining Equations (23) to (26), we get

$$\frac{\partial \mathcal{L}'}{\partial (U'_i)_j} = \begin{cases} \frac{\partial \mathcal{L}'}{\partial (U'_i)_j} E & \text{if } i \text{ odd} \\ \frac{\partial \mathcal{L}'}{\partial (U'_i)_j} F & \text{if } i \text{ even} \end{cases}$$

### A.7.3 First Layer

Through similar derivations as before, we obtain

$$\begin{aligned} \frac{\partial \mathcal{L}'}{\partial S'_{kl}} &= \sum_{ij} \frac{\partial \mathcal{L}'}{\partial (U'_i)_j} \frac{\partial (U'_i)_j}{\partial T'_{kj}} \frac{\partial T'_{kj}}{\partial S'_{kl}} \\ &= \sum_{ij} \frac{\partial \mathcal{L}}{\partial (U_i)_k} \frac{\partial (U_i)_k}{\partial T_{kj}} \frac{\partial T_{kj}}{\partial S_{kl}} \\ &= \frac{\partial \mathcal{L}}{\partial S_{kl}} \end{aligned}$$

and

$$\frac{\partial \mathcal{L}}{\partial \mathbf{W}_{ij}^{(1)}} = \sum_{kl} \frac{\partial \mathcal{L}}{\partial S_{kl}} \frac{\partial S_{kl}}{\partial \mathbf{W}_{ij}^{(1)}} = \sum_{kl} \frac{\partial \mathcal{L}}{\partial S_{kl}} (X_i)_k^\top (X_j)_l$$

This gives us the transformed gradient:

$$\begin{aligned} \frac{\partial \mathcal{L}'}{\partial \mathbf{W}_{11}^{(1)}} &= E^\top \frac{\partial \mathcal{L}}{\partial \mathbf{W}_{11}^{(1)}} E & \frac{\partial \mathcal{L}'}{\partial \mathbf{W}_{12}^{(1)}} &= E^\top \frac{\partial \mathcal{L}}{\partial \mathbf{W}_{12}^{(1)}} F \\ \frac{\partial \mathcal{L}'}{\partial \mathbf{W}_{21}^{(1)}} &= F^\top \frac{\partial \mathcal{L}}{\partial \mathbf{W}_{21}^{(1)}} E & \frac{\partial \mathcal{L}'}{\partial \mathbf{W}_{22}^{(1)}} &= F^\top \frac{\partial \mathcal{L}}{\partial \mathbf{W}_{22}^{(1)}} F \end{aligned}$$

which implies the desired structure.

## B Tight Bound Proof for Theorem 2

### B.1 Summary

To simplify notation within this section, we refer to the parameters  $\alpha_3, \beta_2$ , and  $\gamma_3$ , simply as  $\alpha, \beta$ , and  $\gamma$ , respectively. We show that  $\gamma$  is the first parameter to reach the value  $1/2$  after a time  $T_1 = \Theta(N)$ , then remains bounded. Later,  $\beta$  reaches  $1/2$  after an additional time  $T_2 = \Theta(N^2)$ . Finally,  $\alpha$  reaches  $1/2$  after an additional time  $T_3 = O(N^2)$ . This gives the total times  $T_\alpha = T_1 = \Theta(N)$ ,  $T_\beta = T_1 + T_2 = \Theta(N) + \Theta(N^2) = \Theta(N^2)$ , and  $T_\gamma = T_1 + T_2 + T_3 = \Theta(N) + \Theta(N^2) + O(N^2) = \Theta(N^2)$ . Each step is proven by appropriately bounding the gradient updates. We give the full proof below.

### B.2 Setup

Recall the architecture and loss:

$$U = \left[ X \mid \sigma(XW^{(1)}X^\top)X \right] \quad V = \left[ U \mid \sigma(UW^{(2)}U^\top)U \right]$$

$$z = V_{2N+1}W^{(3)} \quad \mathcal{L} = \|y - z\|^2$$

where  $[\cdot \mid \cdot]$  denotes matrix concatenation, and

$$\begin{aligned} W^{(1)} &\in \mathbb{R}^{2D \times 2D} & W^{(2)} &\in \mathbb{R}^{4D \times 4D} & W^{(3)} &\in \mathbb{R}^{8D \times D} \\ U &\in \mathbb{R}^{(2N+1) \times 4D} & V &\in \mathbb{R}^{(2N+1) \times 8D} & z &\in \mathbb{R}^D \\ X &\in \mathbb{R}^{(2N+1) \times 2D} & y &\in \mathbb{R}^D \end{aligned}$$

We use  $\sigma$  to denote the softmax function with causal masking. We apply a causal mask that prevents a position from attending to itself, which is not a standard practice, but it greatly simplifies the proofs.

The data is generated as:

$$X_{2i-1} = [a_i \mid p_i] \quad X_{2i} = [b_i \mid Mp_i] \quad \forall i \in \{1, \dots, N\}$$

$$X_{2N+1} = [a_q \mid 0] \quad y = b_q$$

where

$$a_i, b_i, p_i \in \mathbb{R}^D \quad q \in \{1, 2, \dots, N\} \quad M = \begin{bmatrix} \mathbf{0} & I \\ I & \mathbf{0} \end{bmatrix}$$

### B.3 Loss Function

We begin by deriving a closed-form expression of the loss in terms of the three parameters.

The orthonormal inputs give us the following attention scores in the first layer:

$$(XW^{(1)}X^\top)_{ij} = \begin{cases} \alpha & i = 2k, j = i - 1 \\ 0 & \text{otherwise} \end{cases}$$

Applying the softmax attention with causal masking gives us:

$$\sigma(XW^{(1)}X^\top)_{ij} = \begin{cases} \frac{e^\alpha}{i-2+e^\alpha} & i = 2k, j = i - 1 \\ \frac{1}{i-2+e^\alpha} & i = 2k, j \neq i - 1 \\ \frac{1}{i-1} & i = 2k + 1 \end{cases}$$

From Assumption 8, the target label is the last element in the sequence, following immediately after the queried item. This means that only the target label will contain the queried item after the first layer. Therefore, the target label will be the only position attended by the query:

$$(UW^{(2)}U^\top)_{2N+1,i} = \begin{cases} \beta \frac{e^\alpha}{2N-2+e^\alpha} & i = 2N \\ 0 & \text{otherwise} \end{cases}$$

Applying the softmax attention gives:

$$\sigma(UW^{(2)}U^\top)_{2N+1,i} = \begin{cases} \frac{s}{s+2N-1} & i = 2N \\ \frac{1}{s+2N-1} & \text{otherwise} \end{cases}$$

where  $s = e^{\beta \frac{e^\alpha}{2N-2+e^\alpha}}$ .

Applying the output projection layer will give us:

$$z = \frac{\gamma}{s + 2N - 1} \left( s b_N + a_N + \sum_{i=1}^{N-1} (a_i + b_i) \right)$$

The final loss will be:

$$\begin{aligned} \mathcal{L} &= \|z - b_i\|^2 = \|z\|^2 - 2z^\top b_i + \|b_i\|^2 \\ &= \gamma^2 \frac{s^2 + 2N - 1}{(s + 2N - 1)^2} - 2\gamma \frac{s}{s + 2N - 1} + 1 \end{aligned}$$

where  $s = e^{\beta \frac{e^\alpha}{2N-2+e^\alpha}}$ .

Note that as long as inputs are orthonormal and the target label is in the last position, the loss only depends on  $\alpha, \beta, \gamma$ , and  $N$ . Any distribution over orthonormal inputs will give the same expected loss.

## B.4 Loss Gradient

We now proceed to compute the partial derivatives of the loss function with respect to each of the three parameters.

### B.4.1 Auxiliary definitions

$$\begin{aligned} G &= e^\alpha + 2N - 2, & F &= 2N - 1, \\ s &= \exp\left(\frac{\beta e^\alpha}{G}\right), & r &= s + F, \\ \mathcal{L} &= \frac{\gamma^2 (s^2 + F)}{r^2} - 2\gamma \frac{s}{r} + 1. \end{aligned}$$

### B.4.2 Partial derivative w.r.t. $\gamma$

$$\begin{aligned} \frac{\partial \mathcal{L}}{\partial \gamma} &= \frac{\partial}{\partial \gamma} \left( \frac{\gamma^2 (s^2 + F)}{r^2} - 2\gamma \frac{s}{r} + 1 \right) \\ &= 2\gamma \frac{s^2 + F}{r^2} - 2 \frac{s}{r} \end{aligned}$$

### B.4.3 Partial derivative w.r.t. $s$

$$\begin{aligned}\frac{\partial \mathcal{L}}{\partial s} &= \frac{\partial}{\partial s} \left( \frac{\gamma^2 (s^2 + F)}{r^2} \right) - 2\gamma \frac{\partial}{\partial s} \left( \frac{s}{r} \right) \\ &= \gamma^2 \frac{2s r^2 - (s^2 + F) 2r \frac{\partial r}{\partial s}}{r^4} - 2\gamma \frac{r - s \frac{\partial r}{\partial s}}{r^2}\end{aligned}$$

But since  $\partial r / \partial s = 1$ ,

$$\begin{aligned}\frac{\partial \mathcal{L}}{\partial s} &= \frac{2\gamma^2 s r - 2\gamma^2 (s^2 + F)}{r^3} - 2\gamma \frac{r - s}{r^2} \\ &= 2F \left( \frac{\gamma^2 (s - 1)}{r^3} - \frac{\gamma}{r^2} \right)\end{aligned}$$

### B.4.4 Derivatives of $s$

$$s = \exp\left(\frac{\beta e^\alpha}{G}\right) \implies \begin{cases} \frac{\partial s}{\partial \alpha} = s \frac{\partial}{\partial \alpha} \left( \frac{\beta e^\alpha}{G} \right) = s \frac{\beta e^\alpha (G - e^\alpha)}{G^2} = s \frac{2(N-1) \beta e^\alpha}{G^2} \\ \frac{\partial s}{\partial \beta} = s \frac{\partial}{\partial \beta} \left( \frac{\beta e^\alpha}{G} \right) = s \frac{e^\alpha}{G} \end{cases}$$

### B.4.5 Applying the chain-rule results

$$\begin{aligned}\frac{\partial \mathcal{L}}{\partial \alpha} &= \frac{\partial \mathcal{L}}{\partial s} \frac{\partial s}{\partial \alpha} = 2F \left( \frac{\gamma^2 (s-1)}{r^3} - \frac{\gamma}{r^2} \right) \times s \frac{2(N-1) \beta e^\alpha}{G^2} \\ &= \frac{4\beta (N-1) F s e^\alpha}{G^2} \left( \frac{\gamma^2 (s-1)}{r^3} - \frac{\gamma}{r^2} \right) \\ \frac{\partial \mathcal{L}}{\partial \beta} &= \frac{\partial \mathcal{L}}{\partial s} \frac{\partial s}{\partial \beta} = 2F \left( \frac{\gamma^2 (s-1)}{r^3} - \frac{\gamma}{r^2} \right) \times s \frac{e^\alpha}{G} \\ &= \frac{2F s e^\alpha}{G} \left( \frac{\gamma^2 (s-1)}{r^3} - \frac{\gamma}{r^2} \right)\end{aligned}$$

### B.4.6 Final results

$$\begin{aligned}\frac{\partial \mathcal{L}}{\partial \alpha} &= \frac{4\beta (N-1) F s e^\alpha}{G^2} \left( \frac{\gamma^2 (s-1)}{r^3} - \frac{\gamma}{r^2} \right) \\ \frac{\partial \mathcal{L}}{\partial \beta} &= \frac{2F s e^\alpha}{G} \left( \frac{\gamma^2 (s-1)}{r^3} - \frac{\gamma}{r^2} \right) \\ \frac{\partial \mathcal{L}}{\partial \gamma} &= 2\gamma \frac{s^2 + F}{r^2} - 2\frac{s}{r}\end{aligned}$$

### B.4.7 Verification

We verify the correctness of the previous results using automated symbolic differentiation with the *SymPy* library. The code is provided with this paper.

## B.5 Emergence of In-Context Learning

Combining the previously obtained loss derivatives with the zero initialization, we obtain the full set of constraints that determine our training trajectory:

$$\alpha(0) = \beta(0) = \gamma(0) = 0$$

$$\frac{\partial \alpha}{\partial t} = \frac{2\beta(2N-2)(2N-1)se^\alpha}{(e^\alpha + 2N-2)^2} \left( \frac{\gamma}{(s+2N-1)^2} - \frac{\gamma^2(s-1)}{(s+2N-1)^3} \right)$$

$$\frac{\partial \beta}{\partial t} = \frac{2(2N-1)se^\alpha}{e^\alpha + 2N-2} \left( \frac{\gamma}{(s+2N-1)^2} - \frac{\gamma^2(s-1)}{(s+2N-1)^3} \right)$$

$$\frac{\partial \gamma}{\partial t} = 2\frac{s}{s+2N-1} - 2\gamma\frac{s^2+2N-1}{(s+2N-1)^2}$$

where  $s = \exp\left(\beta\frac{e^\alpha}{e^\alpha+2N-2}\right)$ .

We are interested in the first time  $t_{\text{ICL}}$  when all three parameters are greater than  $1/2$ . As we show below, the parameters always reach this value in a specific order: first  $\gamma$ , then  $\beta$ , and finally  $\alpha$ .

We find the total time by breaking it down into three different times, one for each parameter:

$$t_{\text{ICL}} = T_1 + T_2 + T_3$$

We show that  $\gamma$  emerges in  $T_1 = \Theta(N)$ ,  $\beta$  emerges after another  $T_2 = \Theta(N^2)$ , and finally  $\alpha$  emerges after another  $T_3 = O(N^2)$ . This gives the total time:

$$t_{\text{ICL}} = \Theta(N) + \Theta(N^2) + O(N^2) = \Theta(N^2)$$

## B.6 Emergence of $\gamma$ in $T_1 = \Theta(N)$

We start in the regime  $0 \leq \alpha, \beta, \gamma < \frac{1}{2}$ . We show that  $\gamma$  is the first to leave this regime at a time  $T_1 = O(N)$ .

### B.6.1 Dynamics of $\gamma$

Using  $\alpha, \beta < \frac{1}{2}$ , we get:

$$s = \exp\left(\beta\frac{e^\alpha}{e^\alpha+2N-2}\right) = 1 + O(1/N)$$

Using  $\gamma < \frac{1}{2}$ , we get:

$$\begin{aligned} \frac{\partial \gamma}{\partial t} &= 2\frac{s}{s+2N-1} - 2\gamma\frac{s^2+2N-1}{(s+2N-1)^2} \\ &\geq 2\frac{s}{s+2N-1} - \frac{s^2+2N-1}{(s+2N-1)^2} \\ &\geq 2\frac{1+O(1/N)}{2N+O(1/N)} - \frac{2N+O(1/N)}{(2N+O(1/N))^2} \\ &\geq \frac{1+O(1/N)}{N} - \frac{2N+O(1/N)}{4N^2} \\ &\geq \frac{1}{2N} + O(1/N^2) \end{aligned}$$

$$\begin{aligned}
\frac{\partial \gamma}{\partial t} &= 2 \frac{s}{s+2N-1} - 2\gamma \frac{s^2+2N-1}{(s+2N-1)^2} \\
&\leq 2 \frac{s}{s+2N-1} \\
&\leq 2 \frac{1+O(1/N)}{2N+O(1/N)} \\
&\leq \frac{1}{N} + O(1/N^2)
\end{aligned}$$

This gives us

$$\frac{\partial \gamma}{\partial t} = \Theta(1/N)$$

Integrating over time, we obtain:

$$\gamma(T_1) = \int_0^{T_1} \frac{\partial \gamma}{\partial t} dt = T_1 \Theta(1/N)$$

Since  $\gamma(T_1) = 1/2$ , we get that  $T_1 = \Theta(N)$ .

### B.6.2 Dynamics of $\alpha$ and $\beta$

We are left to show that the condition  $\alpha, \beta < \frac{1}{2}$  holds until  $T_1$ .

$$\begin{aligned}
\frac{\partial \alpha}{\partial t} &= \underbrace{\frac{2\beta(2N-2)(2N-1)se^\alpha}{(e^\alpha+2N-2)^2}}_{O(1)} \left( \underbrace{\frac{\gamma}{(s+2N-1)^2}}_{O(1/N^2)} - \underbrace{\frac{\gamma^2(s-1)}{(s+2N-1)^3}}_{O(1/N^4)} \right) \\
&= O(1/N^2)
\end{aligned}$$

$$\begin{aligned}
\frac{\partial \beta}{\partial t} &= \underbrace{\frac{2(2N-1)se^\alpha}{e^\alpha+2N-2}}_{O(1)} \left( \underbrace{\frac{\gamma}{(s+2N-1)^2}}_{O(1/N^2)} - \underbrace{\frac{\gamma^2(s-1)}{(s+2N-1)^3}}_{O(1/N^4)} \right) \\
&= O(1/N^2)
\end{aligned}$$

Integrating over time, we get  $\alpha(T_1) = O(1/N)$  and  $\beta(T_1) = O(1/N)$ . Therefore, for large enough  $N$ , it is guaranteed that  $\alpha$  and  $\beta$  will not reach  $1/2$  by the time that  $\gamma$  does.

### B.6.3 Non-negativity

For completeness, we also show that parameters are always increasing within this regime, which guarantees that they will never become negative:

$$\frac{\partial \alpha}{\partial t} = \underbrace{\frac{2\beta(2N-2)(2N-1)se^{\alpha\gamma}}{(e^{\alpha} + 2N - 2)^2}}_{\geq 0} \left( \underbrace{\frac{1}{(s+2N-1)^2}}_{\substack{\Theta(1/N^2) \\ \geq 0}} - \underbrace{\frac{\gamma(s-1)}{(s+2N-1)^3}}_{O(1/N^4)} \right) \geq 0$$

$$\frac{\partial \beta}{\partial t} = \underbrace{\frac{2(2N-1)se^{\alpha\gamma}}{e^{\alpha} + 2N - 2}}_{\geq 0} \left( \underbrace{\frac{1}{(s+2N-1)^2}}_{\substack{\Theta(1/N^2) \\ \geq 0}} - \underbrace{\frac{\gamma(s-1)}{(s+2N-1)^3}}_{O(1/N^4)} \right) \geq 0$$

### B.7 Emergence of $\beta$ after $T_2 = \Theta(N^2)$

We have now entered a new regime where  $0 \leq \alpha, \beta \leq 1/2$  and  $1/2 \leq \gamma \leq 3/2$ . We will show that  $\beta$  is the first to leave this regime after an additional time  $T_2 = \Theta(N^2)$ .

#### B.7.1 Bounding $\gamma$

We begin by showing that  $\gamma$  remains bounded below  $3/2$ . We show that  $\partial\gamma/\partial t$  would be negative at  $\gamma = 3/2$ , which implies that  $\gamma$  will never go above  $3/2$ . We use the fact that  $s = 1 + O(1/N)$  whenever  $\alpha, \beta = O(1)$ :

$$\begin{aligned} \frac{\partial \gamma}{\partial t} &= 2 \frac{s}{s+2N-1} - 2\gamma \frac{s^2 + 2N - 1}{(s+2N-1)^2} \\ &= 2 \frac{s}{s+2N-1} - 3 \frac{s^2 + 2N - 1}{(s+2N-1)^2} \\ &= 2 \frac{1 + O(1/N)}{2N + O(1/N)} - 3 \frac{2N + O(1/N)}{(2N + O(1/N))^2} \\ &= \frac{1 + O(1/N)}{N} - \frac{3N + O(1/N)}{2N^2} \\ &= -\frac{1}{2N} + O(1/N^2) \\ &< 0 \end{aligned}$$

#### B.7.2 Dynamics of $\beta$

Applying the fact that  $\gamma = \Theta(1)$  and  $s = 1 + O(1/N) = \Theta(1)$  gives us:

$$\frac{\partial \beta}{\partial t} = \underbrace{\frac{2(2N-1)se^{\alpha\gamma}}{e^{\alpha} + 2N - 2}}_{\Theta(1)} \left( \underbrace{\frac{1}{(s+2N-1)^2}}_{\Theta(1/N^2)} - \underbrace{\frac{\gamma(s-1)}{(s+2N-1)^3}}_{O(1/N^4)} \right) = \Theta(1/N^2)$$

By integrating, we obtain the value of  $\beta$  after  $T_2$ :

$$\beta(T_1 + T_2) = \beta(T_1) + \int_{T_1}^{T_1 + T_2} \frac{\partial \beta}{\partial t} dt = O(1/N) + T_2 \Theta(1/N^2)$$

This gives us that  $T_2 \Theta(1/N^2) = 1/2$ , which implies that  $T_2 = \Theta(N^2)$ .

#### B.7.3 Dynamics of $\alpha$

For completeness, we must establish that  $\alpha$  does not become greater than  $1/2$  before  $\beta$ . This comes from the fact that  $\beta$  is always increasing at a faster rate than  $\alpha$  in this regime:

$$\frac{\partial \alpha}{\partial t} = \underbrace{\frac{\beta(2N-2)}{e^{\alpha} + 2N - 2}}_{< 1} \frac{\partial \beta}{\partial t}$$

### B.8 Emergence of $\alpha$ in $T_3 = O(N^2)$

We have entered our last regime, which we define using the constraints  $0 \leq \alpha \leq 1/2$ ,  $1/2 \leq \gamma \leq 3/2$ , and  $1/2 \leq \beta \leq 20$ .

We know from before that  $\gamma$  remains constrained when  $\alpha, \beta = \Theta(1)$ . We are left to prove that  $\alpha$  becomes greater than  $1/2$  in a time  $T_3 = O(N^2)$  and it does so before  $\beta$  becomes greater than the value 20 (chosen arbitrarily to simplify the proofs).

#### B.8.1 Dynamics of $\alpha$

We establish an upper bound on  $T_3$  using a lower bound on  $\partial\alpha/\partial t$ :

$$\begin{aligned} \frac{\partial\alpha}{\partial t} &= 2\gamma\beta e^\alpha \underbrace{\frac{(2N-2)(2N-1)s}{(e^\alpha + 2N-2)^2}}_{1+O(1/N)} \left( \underbrace{\frac{1}{(s+2N-1)^2}}_{1/(4N^2)+O(1/N^3)} - \underbrace{\frac{\gamma(s-1)}{(s+2N-1)^3}}_{O(1/N^4)} \right) \\ &> \frac{1}{8N^2} + O\left(\frac{1}{N^3}\right) \end{aligned}$$

Integrating over time gives:

$$\begin{aligned} \alpha(T_1 + T_2 + T_3) &= \alpha(T_1 + T_2) + \int_{T_1+T_2}^{T_1+T_2+T_3} \frac{\partial\alpha}{\partial t} dt \\ &> T_3 \left( \frac{1}{8N^2} + O\left(\frac{1}{N^3}\right) \right) \end{aligned}$$

Applying that  $\alpha(T_1 + T_2 + T_3) = 1/2$  gives us  $T_3 < 4N^2 + O(1/N) = O(N^2)$ .

#### B.8.2 Dynamics of $\beta$

Finally, we must show that  $\beta$  does not reach 20 during  $T_3$ . We achieve this using an upper bound on  $\partial\beta/\partial t$ :

$$\begin{aligned} \frac{\partial\beta}{\partial t} &= 2e^\alpha \gamma \underbrace{\frac{(2N-1)s}{e^\alpha + 2N-2}}_{1+O(1/N)} \left( \underbrace{\frac{1}{(s+2N-1)^2}}_{1/(4N^2)+O(1/N^3)} - \underbrace{\frac{\gamma(s-1)}{(s+2N-1)^3}}_{O(1/N^4)} \right) \\ &< \frac{3\sqrt{e}}{4N^2} + O(1/N^3) \end{aligned}$$

Integrating over time gives:

$$\begin{aligned} \beta(T_1 + T_2 + T_3) &= \beta(T_1 + T_2) + \int_{T_1+T_2}^{T_1+T_2+T_3} \frac{\partial\beta}{\partial t} dt \\ &< \frac{1}{2} + T_3 \left( \frac{3\sqrt{e}}{4N^2} + O\left(\frac{1}{N^3}\right) \right) \\ &< \frac{1}{2} + \left( 4N^2 + O(1/N) \right) \left( \frac{3\sqrt{e}}{4N^2} + O\left(\frac{1}{N^3}\right) \right) \\ &< \frac{1}{2} + 3\sqrt{e} + O(1/N) \\ &< 5.45 + O(1/N) \\ &< 20 \end{aligned}$$

### C Training Details and Additional Figures for Section 3.2

We confirm our theoretical result by visualizing the weights during standard training with stochastic gradient descent. We use learning rate  $\lambda = 1$  and batch size  $B = 512$ .

We sample  $q \sim \text{unif}\{1, N\}$ , and we sample items, labels, and positional embeddings from a multivariate Gaussian:

$$\begin{aligned} (\mathbf{a}_i)_j &\sim \mathcal{N}(0, 1), & (\mathbf{b}_i)_j &\sim \mathcal{N}(0, 1), \\ (\mathbf{p}_i)_j &\sim \mathcal{N}(0, 1), \end{aligned}$$

for all  $i \in \{1, \dots, N\}$  and  $j \in \{1, \dots, D\}$ .

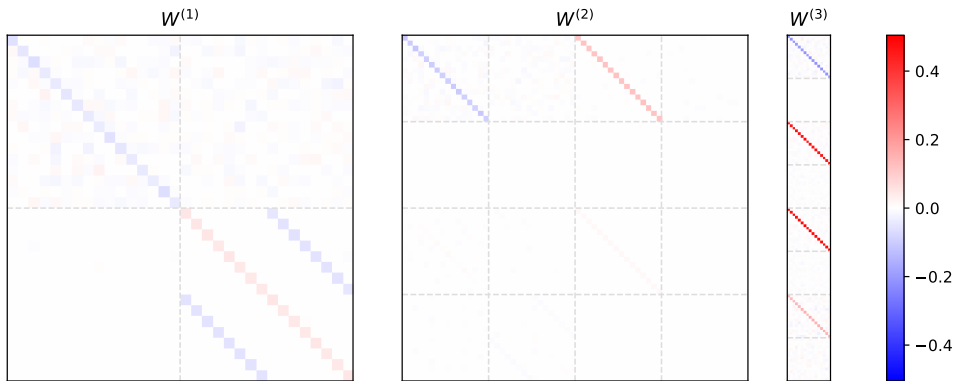


Figure 9: Model weights after 100 training steps with  $D = 16$  and  $N = 4$ .

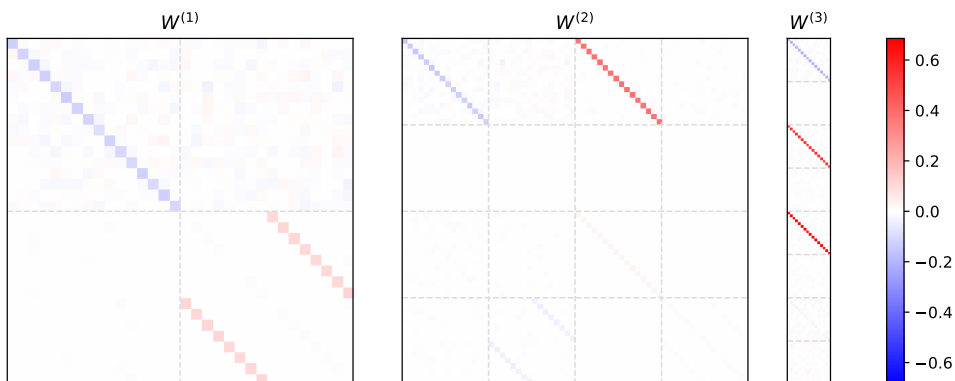


Figure 10: Model weights after 200 training steps with  $D = 16$  and  $N = 4$ .

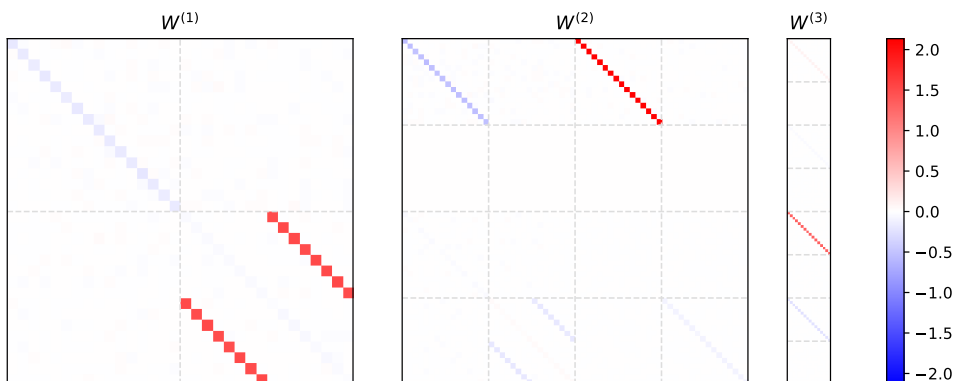


Figure 11: Model weights after 400 training steps with  $D = 16$  and  $N = 4$ .

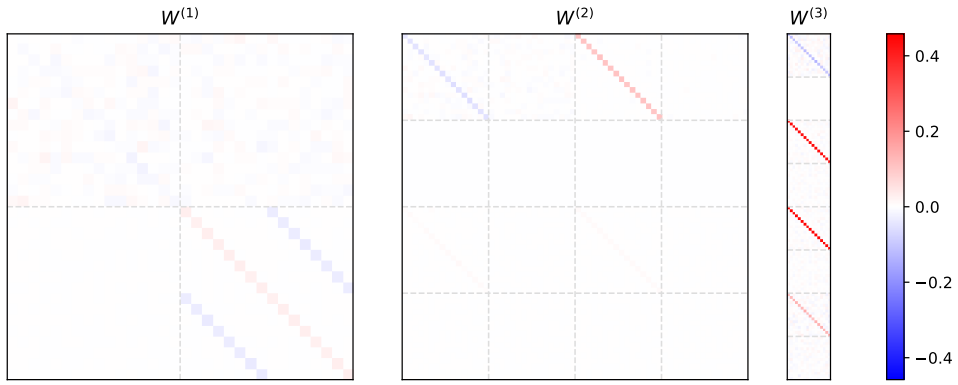


Figure 12: Model weights after 200 training steps with  $D = 16$  and  $N = 8$ .

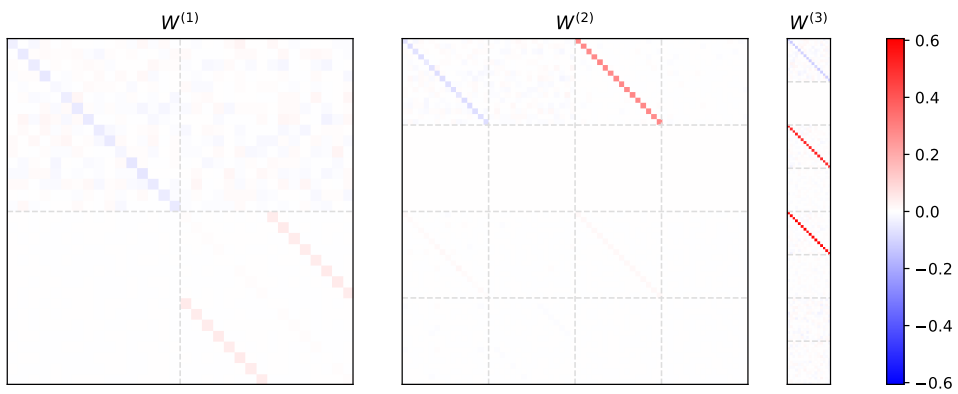


Figure 13: Model weights after 400 training steps with  $D = 16$  and  $N = 8$ .

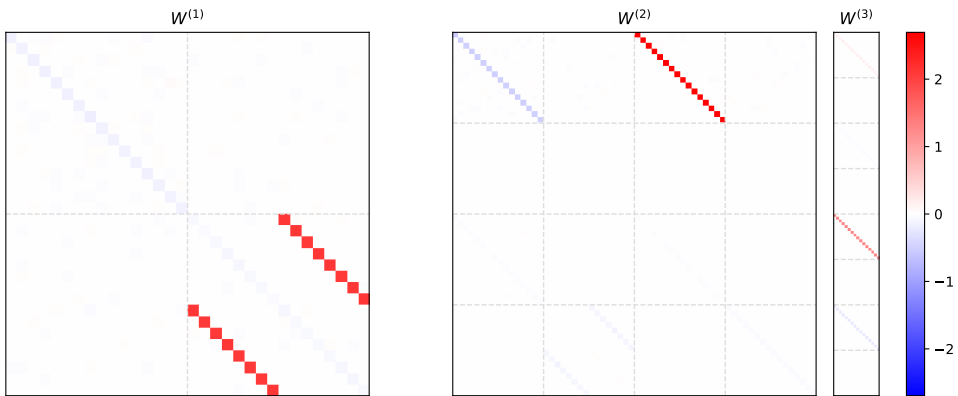


Figure 14: Model weights after 800 training steps with  $D = 16$  and  $N = 8$ .

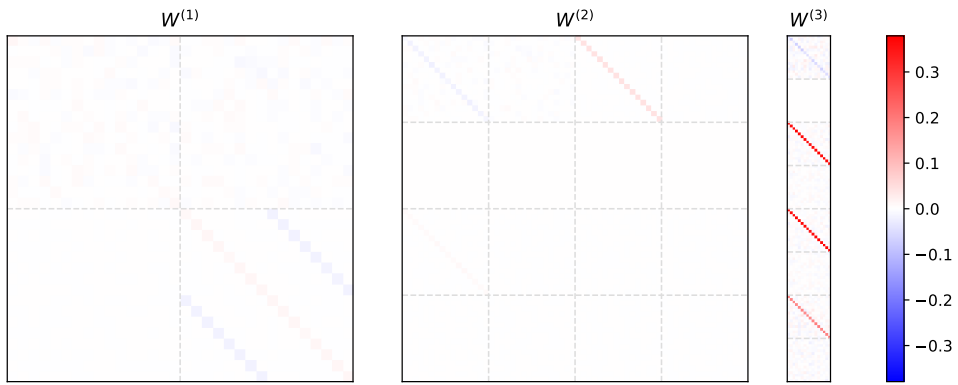


Figure 15: Model weights after 250 training steps with  $D = 16$  and  $N = 16$ .

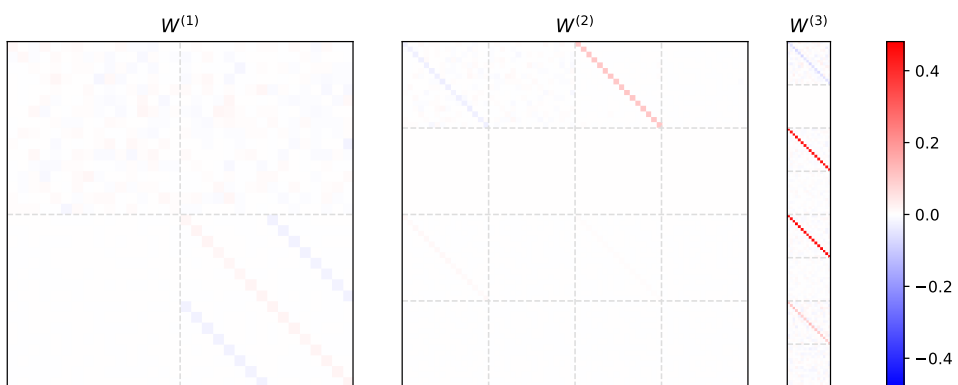


Figure 16: Model weights after 500 training steps with  $D = 16$  and  $N = 16$ .

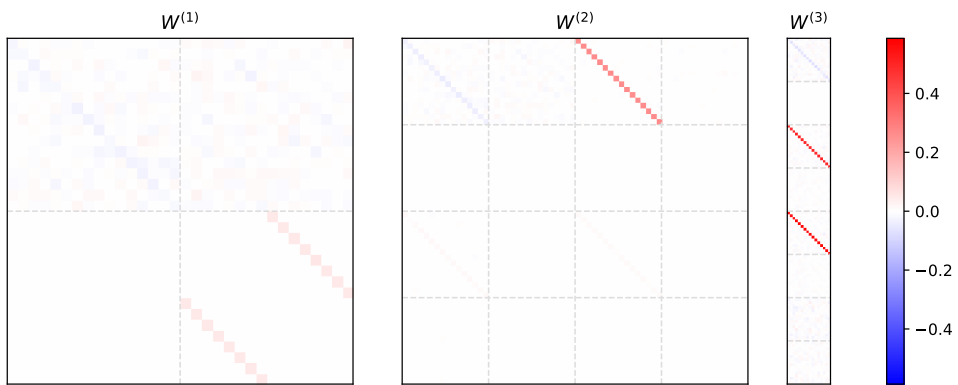


Figure 17: Model weights after 1000 training steps with  $D = 16$  and  $N = 16$ .

## D Training Dynamics

As in the main paper, we visualize the pseudo-parameters and loss during standard training, as well as when training only  $\alpha_3$ ,  $\beta_2$ , and  $\gamma_3$ . We use  $D = 32$ ,  $N = 16$ , learning rate  $\lambda = 1$ , and batch size  $B = 256$ . We determine the value of each pseudo-parameter by measuring the magnitude of the parameter vector along the corresponding component.

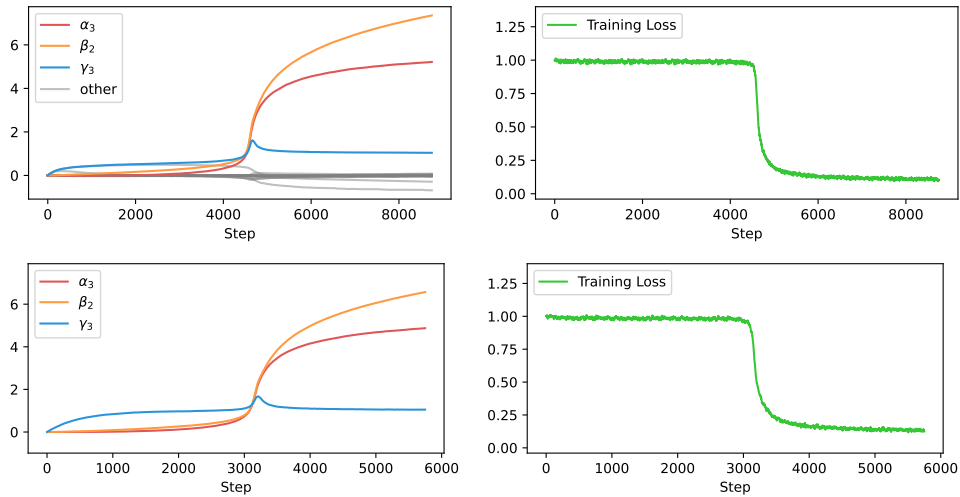


Figure 18: The pseudo-parameters and training loss during training with  $D = 16$  and  $N = 32$ . *Top.* Standard training. *Bottom.* Training only  $\alpha_3$ ,  $\beta_2$ , and  $\gamma_3$ .

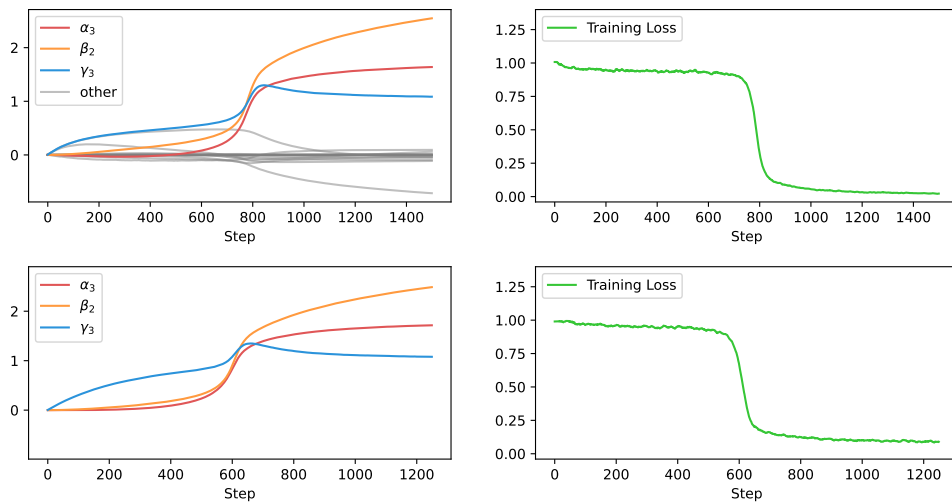


Figure 19: The pseudo-parameters and training loss during training with  $D = 32$  and  $N = 8$ . *Top.* Standard training. *Bottom.* Training only  $\alpha_3$ ,  $\beta_2$ , and  $\gamma_3$ .

## E Training Details for Section 4

We train two transformers, a smaller that is used to visualize the weight structure and a larger that is used to visualize the training dynamics.

For visualizing the weight structure in Figure 3, we use token and positional embeddings with a vocabulary size of 32, a block size of 32, and an embedding dimension of 2048. Since we have only one head per layer, the head dimension is also 2048. We do not use normalization or weight tying. Following standard practice, we train with AdamW (Loshchilov and Hutter, 2017) with learning rate 0.001 and weight decay 0.01. We train for 300 steps with 512 sequences per step. Every sequence has length 17 (8 item-label pairs and one query item) and is placed at a random position in the block. We generate new random sequences for every gradient step as follows: we choose 16 distinct tokens from our vocabulary and group them in item-label pairs; we choose one of the items to be the query; we use the corresponding label as the target output. We construct the input sequences of length 17 by joining the item-label pairs followed by the query item. We use the negative log-likelihood loss applied only at the final position (the query item).

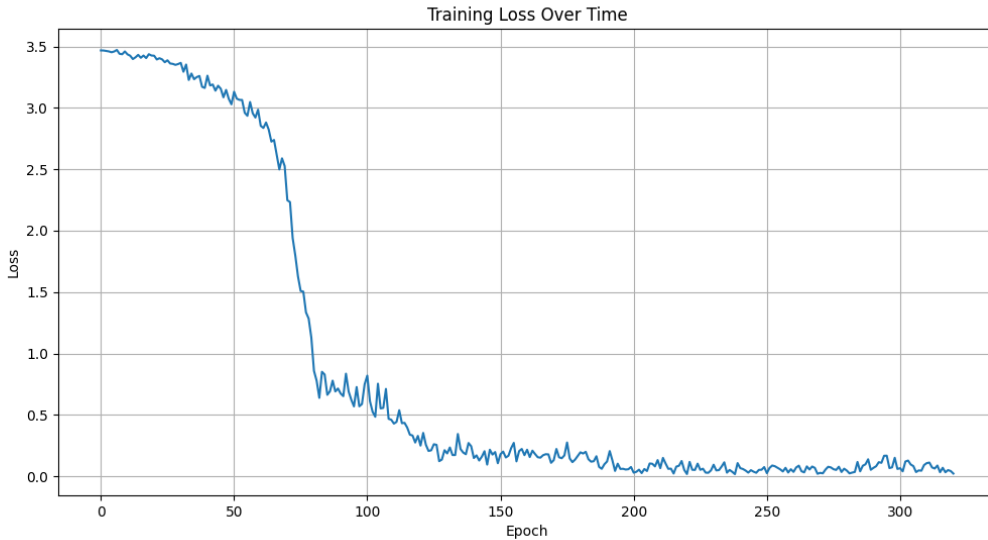


Figure 20: Training loss for the transformer used in Figure 3. Note that every batch is generated independently, hence the training loss is also a test loss.

For visualizing the progress measures during training in Figure 8, we use token and positional embeddings with a vocabulary size of 64, a block size of 64, and an embedding dimension of 4096. The head dimension is also 4096. We use AdamW with learning rate 0.0001 and no weight decay, and batch size 4096. Every sequence has length 33 (16 item-label pairs and one query item).

## F Training Details for Section 3.4

We empirically validate our theoretical results by measuring the emergence times for different values of  $N$ . We find that emergence times are in accordance with theoretical predictions. Results are plotted in Figure 6. We use  $D = 256$ ,  $B = 64$ ,  $\lambda = 100$ . Following our theoretical assumptions, we use orthonormal inputs, zero initialization, and  $q = N$ . We constrain the parameters to the 3-dimensional space spanned by  $\alpha_3$ ,  $\beta_2$ , and  $\gamma_3$ .